FACE PUMPED LASER

Second

Semi-Annual Technical Summary Report

1 June 1965 - 30 November 1965

ONR Contract No. Nonr-4659(00)
Project Code No. 4730
ARPA Order No. 306

Prepared for

Office of Naval Research
Department of Navy
Washington 25, D.C.

Prepared by

Research and Development Center
General Electric Company
Schenectady, N.Y. 12301

GENERAL ELECTRIC

FACE PUMPED LASER

Second
Semi-Annual Technical Summary Report

1 June 1965 - 30 November 1965

Program Manager

Dr. J. C. Almasi

Contributors:

J. P. Chernoch
Dr. W. S. Martin
Dr. K. Tomiyasu

ONR Contract No. Nonr-4659(00)
Project Code No. 4730
ARPA Order No. 306

Prepared for

Office of Naval Research
Department of Navy
Washington 25, D. C.

Prepared by

Research and Development Center
General Electric Company
Schenectady, New York 12301

Submitted by

Heavy Military Electronics Dept.
General Electric Company
Syracuse, New York

This research is part of Project DEFENDER under the joint sponsorship of the Advanced Research Projects Agency, the Office of Naval Research, and the Department of Defense.

AVAILABILITY OF COPIES

U. S. Government agencies with the exception of the Clearing House for Federal Scientific and Technical Information-Department of Commerce (formerly O. T. S.), may obtain copies of this report directly from the Defense Documentation Center. To afford time for patent consideration and filing, release of this report to the Clearing House for Scientific and Technical Information-Commerce Department, or other qualified non-government D. D. C. users prior to one year from the date of the report requires the prior written permission of the General Electric Company - Research and Development Center - 1 River Road, Schenectady, New York, 12301.

TABLE OF CONTENTS

LIST OF ILLUSTRATIONS

LIST OF ILLUSTRATIONS (Continued)

SECTION I

SUMMARY

During the preceding period, several sources were contacted again to seek the latest information on the availability of high quality neodymium-doped glass of sizes sufficiently large to fabricate discs. As a result, two orders were placed on American Optical Company to purchase 3-inch diameter discs made from AOLux #3835 glass and from a special melt of Nd-doped alkali silicate glass.

Refined analyses and measurements have shown that the thermal effects due to pumping at 27,000 joules causes the 6-inch diameter 1-inch thick Nd-doped glass disc to warp with a radius of curvature of 3.7×10^5 cm. With this warpage the out-of-plane displacement of the disc is about 3/4 wavelength at 1.06 μ.

From previous measurements the amount of non-uniformity in the optical thickness due to non-uniformity in pumping, was less than $\lambda/8$ at 1.06 μ across the 6"D disc. Refined measurements have shown that the non-uniformity is less than $\lambda/13$. Both experiments were time integrated measurements.

Amplified spontaneous emission measurements were made on the 6"D 1" thick disc with different conditions on the fine ground cylindrical surface. The results indicate that amplified spontaneous emission is not a limiting factor in the present designs of disc lasers.

Optical coupling and pumping measurements were carried out on the 3-inch disc pump assembly. After many flashes, with 9000 joules and using ultraviolet and infrared filters, there was no measurable damage to the 1.06 μ high reflective mirror.

A preliminary analysis has been carried out on the amount of distortion or deformation permissible in a plane-parallel mirror high Fresnel number Fabry-Perot resonator before the losses introduced become significant.

Single disc oscillator experiments were carried out with 5 different Nd-doped glasses. Laser action was demonstrated with 3 of them. However, due partly to the poor optical quality of the glass discs and partly to the optical finish, laser action could not be obtained across the entire face on any of the discs.

Tipped etalons offer the possibility of mode selection at high power levels. An analysis was carried out investigating the various parameters affecting the design of such mode selectors.

SECTION II

WORK PERFORMED

A. LASER MATERIALS

PROCUREMENT

Another survey was made to determine availability of neodymium-doped glass for the present face pumped laser program. The sources contacted and remarks are given below.

1. Bausch & Lomb Optical Company

Laser glass is available in only laboratory quantities.

2. Chance Pilkington Optical Works

Contact was made through Adolf Meller Company, Providence, R. I. The U. S. distributor is Alfa American Corporation, Rockford, Ill. The barium silicate laser glass contains two percent by weight of Nd_2O_3. The fluorescence lifetime is 620 μsec. A fairly high threshold of 80 to 100 joules is quoted and the 1.06 μ absorption is about 0.4 percent/cm. A laser slab was available but the laser performance of samples from the slab was unknown. The cost was quite exhorbitant compared to that from another commercial source.

3. Corning Glass Works

The Corning #0580 4.7 percent Nd_2O_3 soda lime silicate laser glass has a lifetime of 320 μsec and a 1.06 μ absorption of 0.6 percent/cm. Large sizes of laser glass were not available, and in the meantime Corning Glass Works announced discontinuation of the manufacture of laser glass.

4. Ohara Optical Glass Manufacturing Company

Through the U. S. distributor Chicago Aerial Industries, it was learned that Ohara Optical Glass Manufacturing Company produces neodymium-doped laser glass with Nd_2O_3 content of 0.5, 1, 2, and 5 wt. percent. The fluorescent lifetimes and laser thresholds are unavailable. Large sizes of laser glass were not available.

5. Pittsburgh Plate Glass Company

Some neodymium-doped laser glass was being investigated at the Research Laboratory of Pittsburgh Plate Glass Company, and nothing was available commercially.

6. Schott Glass Works

The U. S. distributor for Schott Glass Works is Fish-Schurman Corporation in New Rochelle, New York. Two neodymium-doped laser glasses are commercially available. Both contained 2 wt. percent Nd_2O_3; one had a fluorescence lifetime of 150 μsec lifetime and the other 80 μsec. A new glass, type LG-55 containing 5 wt. percent Nd_2O_3 has a 600 μsec lifetime. Another glass under development, type LG-3 contains 3 wt. percent Nd_2O_3.

7. Eastman Kodak Company

Eastman Kodak Company has neodymium-doped borate and ND-11 silicate laser glasses. A maximum lifetime of 360 μs can be obtained from 2 wt. percent Nd_2O_3 ND-11 glass.

8. American Optical Company

An order was placed on American Optical Company for two 3" diameter 1-cm thick discs of AOLux #3835 laser glass. This 5 wt. percent Nd_2O_3 silicate glass has a fluorescence lifetime of 500 μsec. The discs were coated 100 percent reflection on one face and low reflection on the other. One face per disc was specified to be flat within $\lambda/10$, however none of the four faces on the two discs met this specification. The discs have been returned for rework.

Another order was placed on American Optical Company for a special melt of neodymium-doped alkali silicate glass with a fluorescence lifetime of at least 800 μsec. Three inch diameter discs will be prepared from this melt.

B. THERMAL EFFECTS

WARPAGE

1. Experimental

Due to the fact that most of the pumping radiation is absorbed near the face of the disc closest to the radiation source, non-uniform heating across the thickness will occur with a concomitant disc warpage. During the preceding period, an analysis showed the amount of warpage to be quite small. An attempt to measure the warpage was unsuccessful due to experimental difficulties. During the present period an improved experiment was carried out and this shows that the warpage is indeed quite small.

In the improved experiment a transparent optical flat was placed on top of the laser disc. An interference pattern was generated by multiple reflections between the adjacent surfaces. By employing a source of illumination with a rather limited coherence length (as contrasted with a gas laser with extremely long coherence length), only the interference between the two faces in close proximity is observed. Thus the measurement is greatly simplified. A commercial (Lapmaster) helium light source designed for flatness measurements was used and this generated a narrow spectral line at 5875 Å.

A photograph of the general arrangement is shown in Fig. B1. The 6"D 1" thick 2% Nd EK ND-11 glass laser disc is mounted in a 1" thick aluminum plate. This plate is mounted above a larger micalex plate; the six flash lamps are mounted on the bottom of the micalex plate. The 6"D reference optical flat is placed on the laser disc; the reference is flat within $\lambda/10$. The helium light is emitted from the inclined panel above the optical flat. An inclined mirror is used to enable viewing the interference fringes horizontally.

A different view of the experimental setup is shown in Fig. B2. The interference fringes created between the close adjacent faces can be seen in the inclined mirror.

In order to increase the input energy to the six EG&G FX-47 flash lamps the circuit was rewired. Each pair of lamps was connected in series and energized by a capacitor bank. The three pairs of lamps with separate capacitor banks were fired simultaneously. This arrangement permitted operation at a higher voltage, and for the same capacitance a higher input energy to the lamps.

The operational procedure for measuring the warpage is to photograph the disc at various times. Figure B3 shows such a series of photographs which we will distinguish by reference to the time at which they were taken. Thus photograph -5 minutes refers to the first picture in Fig. B3 which was

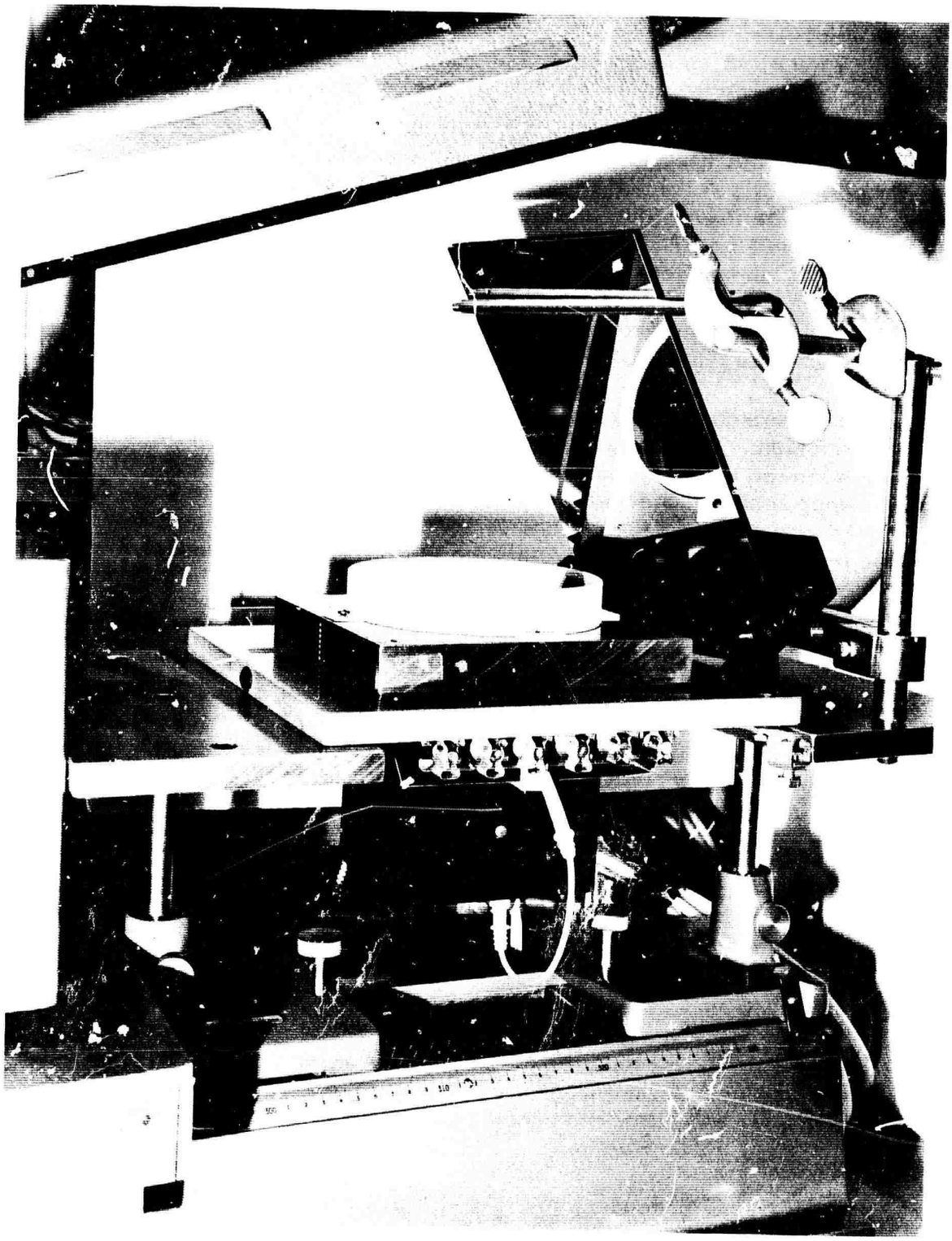

Figure B1. Disc Warpage Experimental Setup

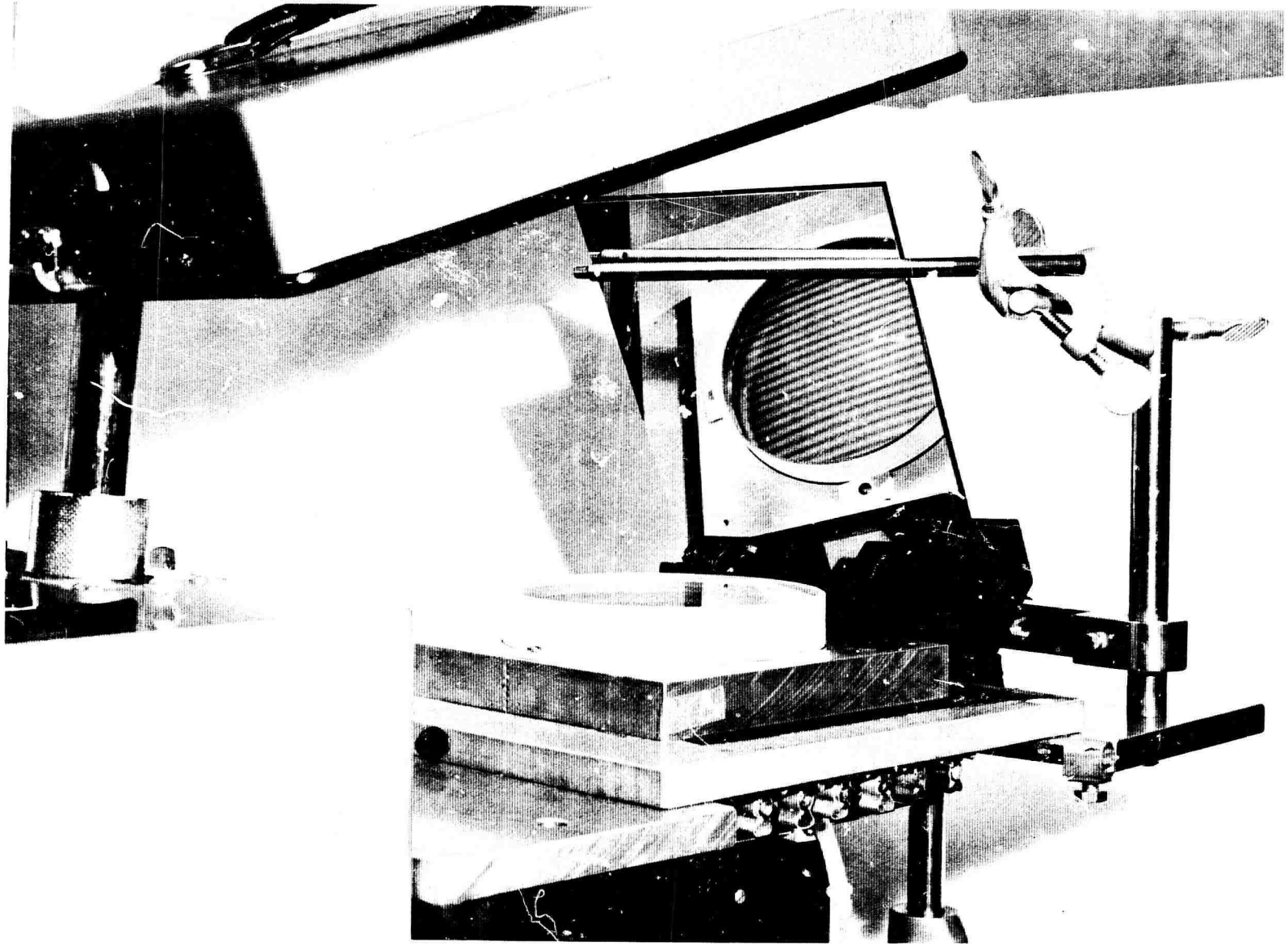

Figure B2. Another View of Warpage Experiment Showing Fringes

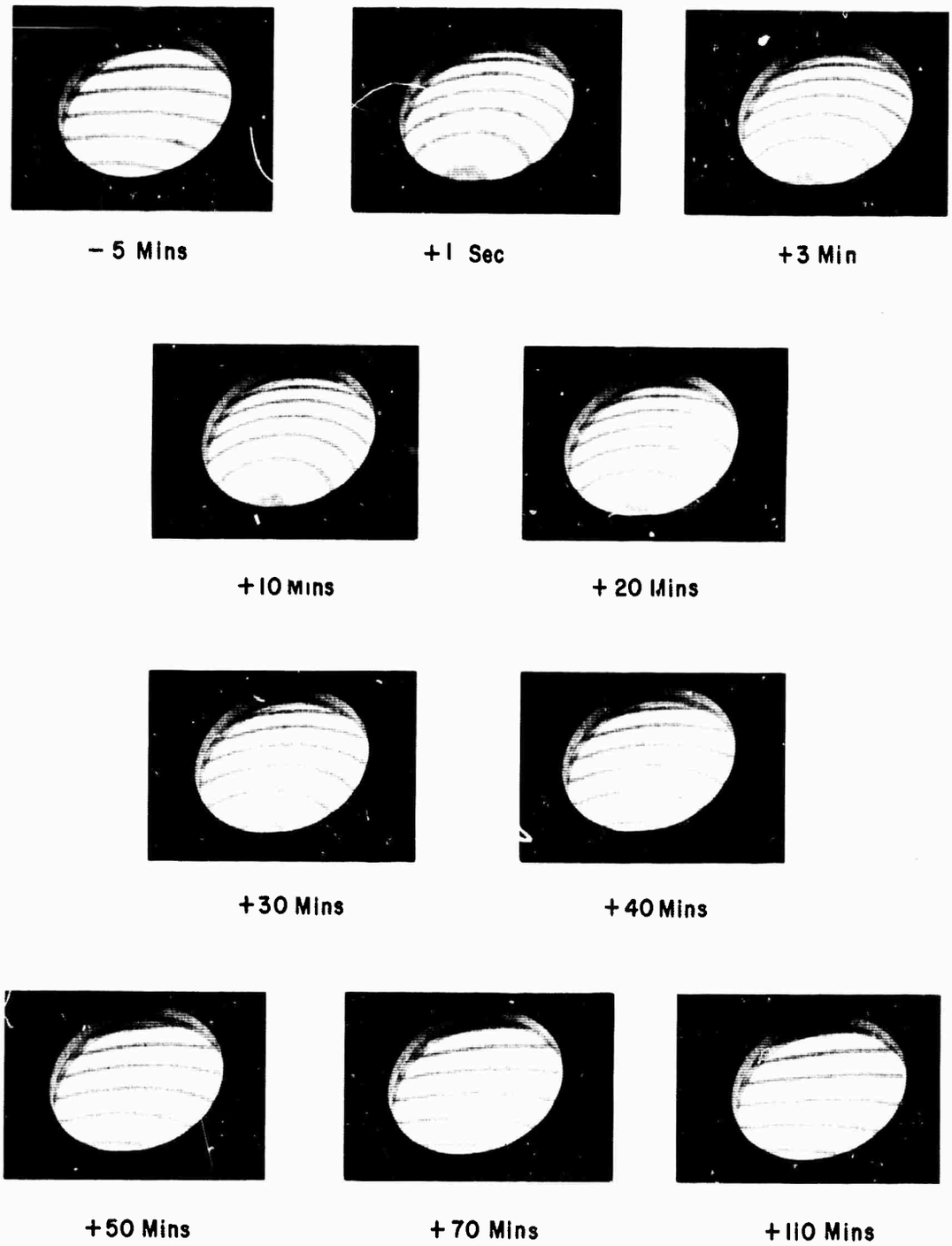

Figure B3. Interferograms as a Function of Time for 15,000 Joules of Stored Pump Energy

taken five minutes before triggering the pump pulse. Comparison of photographs -5 minutes and +1 second shows the sudden shift in fringes which results from warpage caused by the pump pulse. A series of additional photographs over a period of an hour allows us to follow the progressive relaxation of the warpage until it is negligible. A comparison is made between the first photograph after the pump pulse (e. g. +1 second) and a photograph one or two hours later (e. g. +110 minutes) inasmuch as there is sometimes a small shift in the position of the laser disc relative to the reference flat due to shock from the pump pulse (cf. -5 minutes and +110 minutes).

A measurement of warpage was made when the disc was pumped at about 22,000 joules which was the highest energy stored in the capacitor bank used in this experiment. Figure B4 shows the interference patterns ~1 second after the pump pulse and 95 minutes later respectively. Figure B5 shows the method of data reduction. The solid lines in Fig. B5 give a magnified picture of the dark fringes in the interferogram marked ~1 second in Fig. B4. The dashed lines give a similarly scaled picture of the dark fringes in the interferogram marked +95 minutes in Fig. B4. These fringes arise because of a small wedge angle between the laser disc and the reference flat caused by dust between them. The dotted line in Fig. B5 is drawn through the points where the positions of the fringes are stationary. These points represent positions where the optical thickness between the two surfaces does not change. Thus the dotted line represents the locus of stationary optical separation between the surfaces.

Because of the non-normal viewing angle, the outline of the circular disc appears to be elliptical in shape. In Fig. B5, not only the disc outline but also the dotted line appears elliptical. The latter indicates that the warping of the disc is spherical. The fact that the dotted line ellipse is not centered with the outline of the disc indicates that the supporting points of the optical flat do not lie on a circle concentric with the laser disc. A schematic representation of the relationship among interference fringes, supporting points and disc warpage is shown in Fig. B6.

The amount of fringe shift caused by disc warpage can be determined by referring to Fig. B5. It should be noted that the fringe shift is relative to the constant separation locus and not the total out-of-plane displacement for the full diameter of the laser disc. However the radius of curvature R is constant over the entire face of the warped laser disc. The geometrical situation is illustrated schematically in Fig. B7. The radius of curvature $\underline{R}$ is related to the fractional fringe shift $\underline{f}$ and disc surface displacement $\underline{m}$ through the following formulas where the symbols are defined in Fig. B7:

$$m = \frac{r\phi}{2} \qquad \text{(B1)}$$

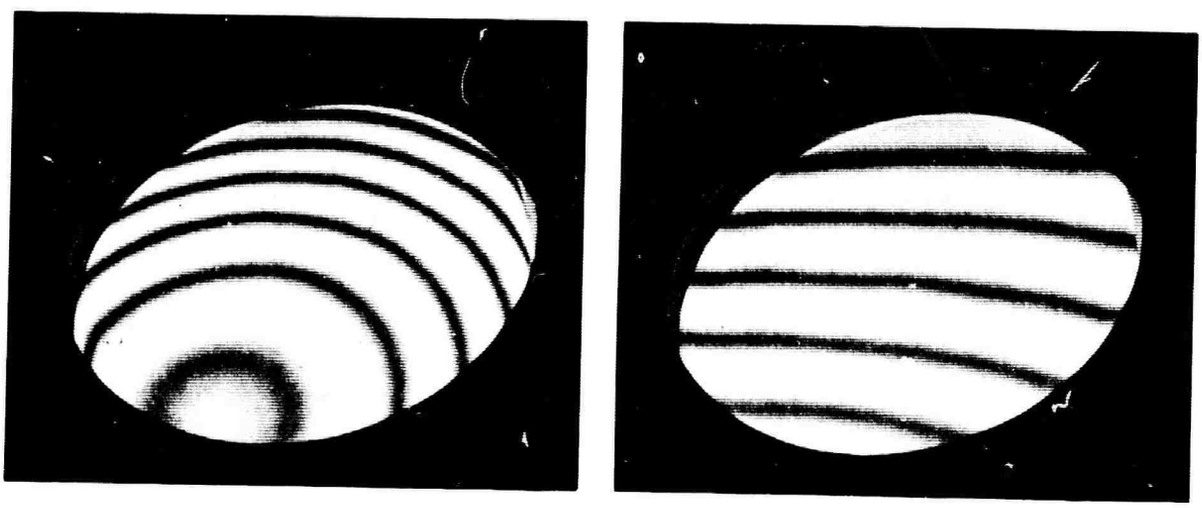

Figure B4. Interferograms to Measure Disc Warpage at 22,000 Joules

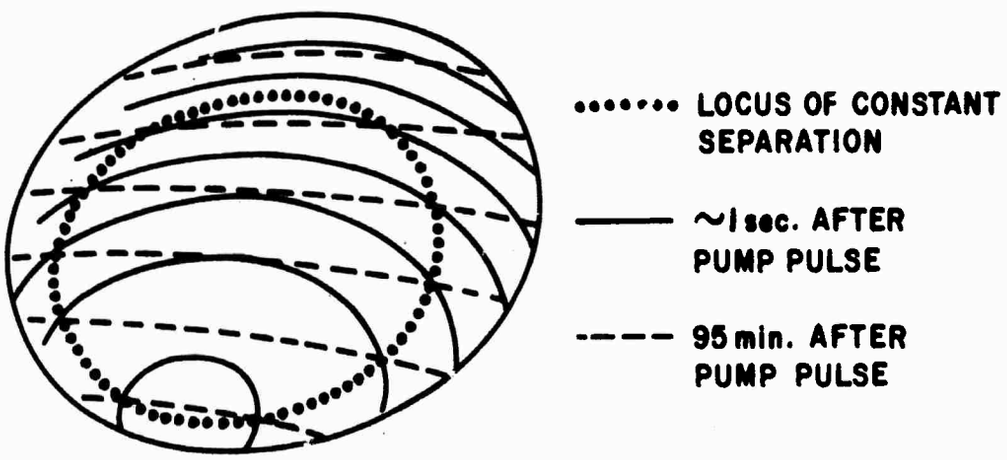

Figure B5. Data Reduction from Fringe Shift

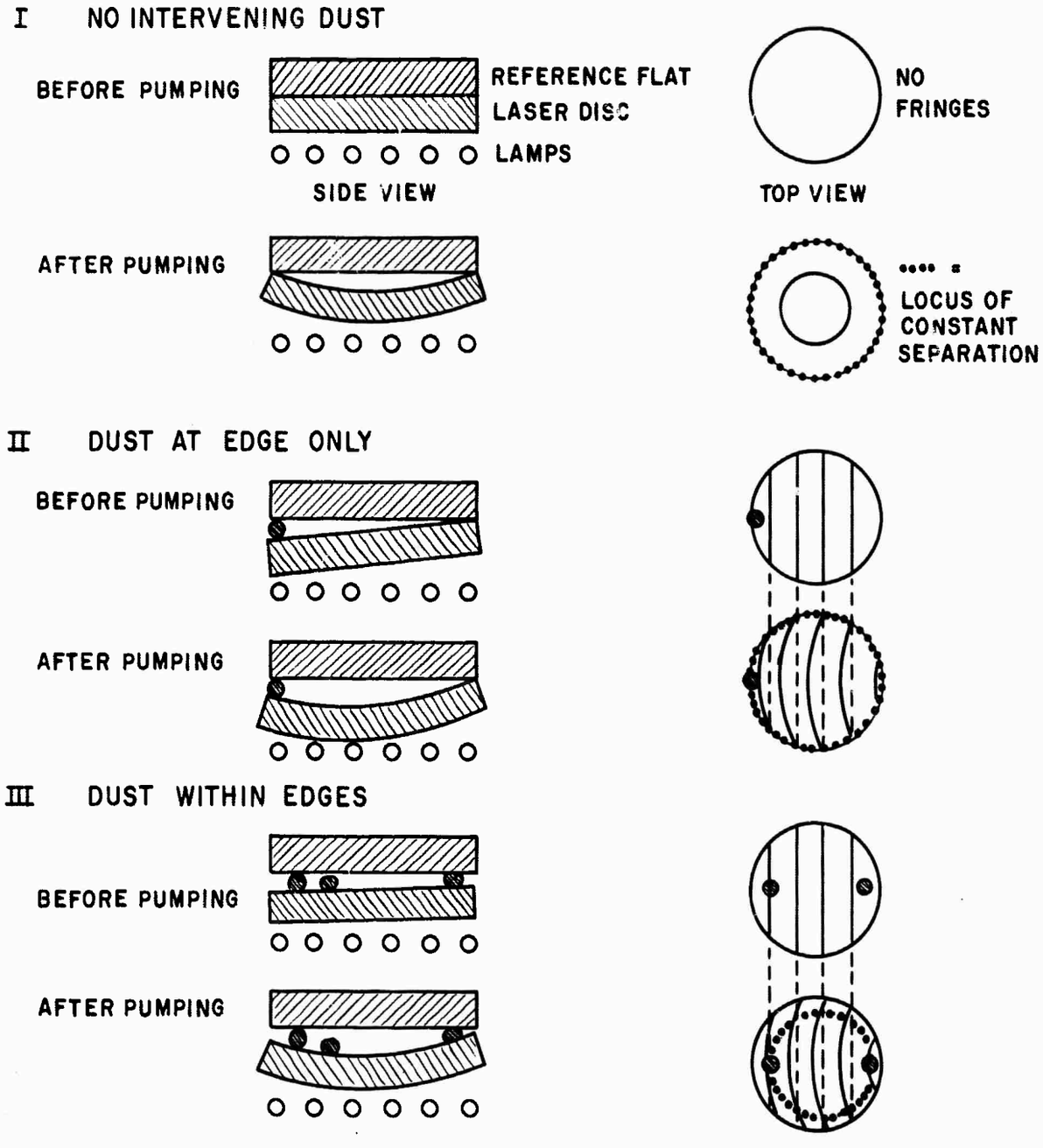

Figure B6. Relationship of Fringes and Dust between Discs

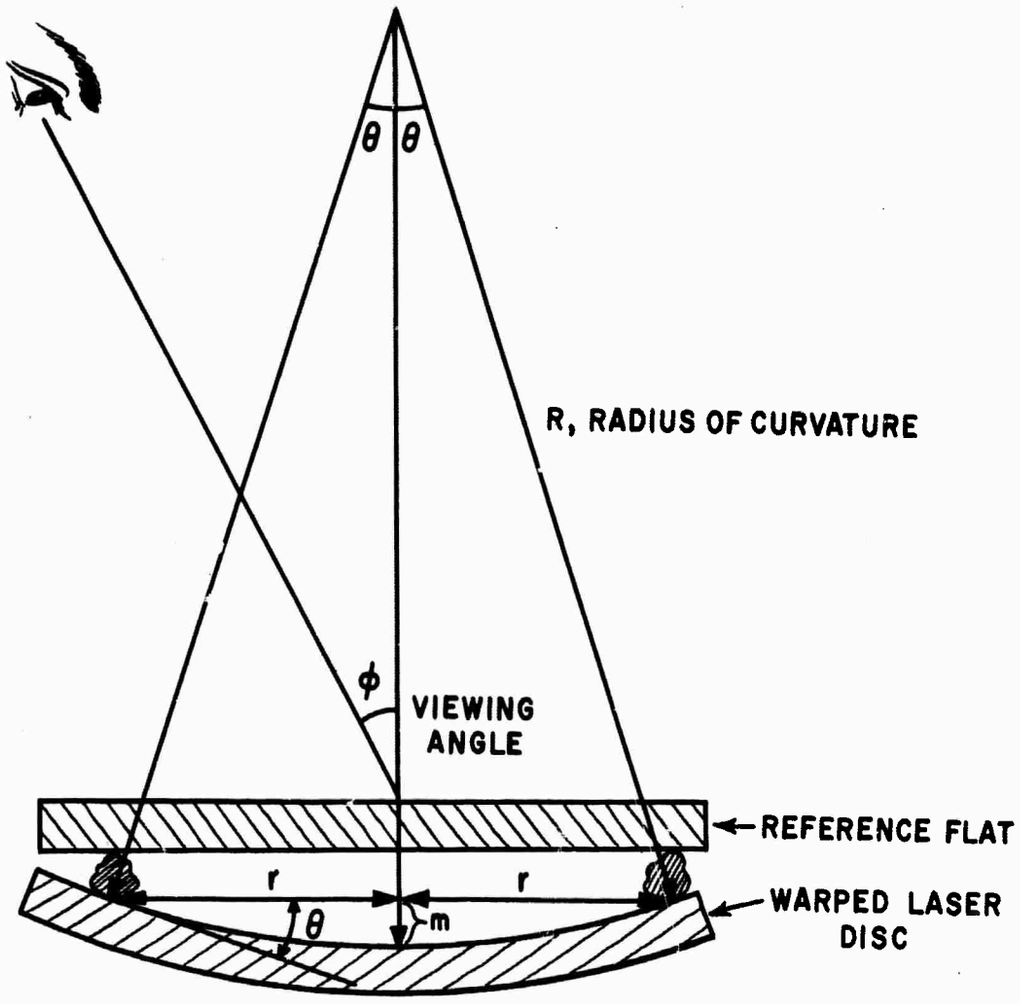

Figure B7. Schematic Drawing Defining Symbols for Warped Disc

$$f = \frac{m \cos \phi}{\lambda/2} \tag{B2}$$

$$r = R\sin\phi \sim R\phi \tag{B3}$$

Combining Eqs. B1, B2, and B3 we find

$$R = \frac{r^2 \cos\phi}{\lambda f} \tag{B4}$$

The amount of pump energy used to obtain the composite interferograms in Fig. B5 was 22,000 joules. The viewing angle ϕ can be determined from the ellipticity of the disc outline, and for this example, $\phi \doteq 39.5^{o}$. Thus from Fig. B5

$$\cos \phi = 0.77$$

$$r = 5.6 \text{ cm}$$

$$f = 0.9 \text{ fringe}$$

With $\lambda = 0.5875 \times 10^{-4}$ cm, the radius of curvature is

$$R = 4.6 \times 10^{5} \text{ cm} = 4600 \text{ meters}$$

With this curvature, the out-of-plane displacement at the center of the laser disc is

$$0.6 \times 10^{-4} \text{ cm}$$

This value is about 0.6λ at 1.06 micron wavelength.

The same experiment was repeated seven times for various energies spanning the ranges of 5000 to 22,000 joules of stored energy in the capacitor bank. As expected, the fringe shifts increase approximately linearly with energy. We may summarize our results for the radius of curvature R as a function of the energy stored in the capacitor bank J (in joules) with the following formula:

$$R \simeq \frac{10^{10}}{J}, \text{ cm.} \tag{B5}$$

2. Comparison of Experiment and Theory

Theoretical calculations previously carried out[(B1)*] for the disc in question predicted a radius of curvature of 3.7×10^{5} cm for an effective lamp temperature of 8000°K for a pulse length of one millisecond. An approximate equivalent black body temperature of 8000°K has been given for an EG&G FX-47 lamp operated at a peak current of 3000 amps delivered in a 500 μsec long

*References are found in Part H

pulse from a 500 μf network charged to 3 kv. For six such lamps, the input energy is 13,500 joules in 500 μsec. If we have the same effective black body temperature (8000°K) but deliver the corresponding power for one millisecond then we expect to require twice as much lamp input energy or ~27,000 joules. Therefore we calculate by using Eq. B5 that an input energy of 27,000 joules will result in a radius of curvature of $\sim 3.7 \times 10^5$ cm. Our empirical formula yields a value of R of 10^{10} cm/27,000 = 3.7×10^5 cm. This agreement is remarkable.

3. Consequences of Disc Warpage

A warped disc acts like a slightly divergent lens but this effect can be ignored if it causes less divergence than that arising from diffraction of the disc aperture. From simple trignonometry and Snell's Law we find that transmission through a warped disc deflects the propagation direction through an angle ϵ as illustrated in Fig. B8. If ϕ (= r/R) is extremely small, the value of ϵ is given by the following equation provided $\phi \ll 1$:

$$\epsilon = \frac{d}{R}\left(\phi + \frac{r}{R}\right)\left(1 - \frac{1}{n}\right)$$

where

d = thickness of disc

R = radius of curvature of the warped disc

ϕ = angle of incidence relative to the normal at the center of the disc

r = radius at intersection of incident ray with disc face

n = index of refraction of disc

The maximum value of ϵ will occur when r = a, the radius of the disc, and for r = a the value of ϵ_{max} will depend on the angle of incidence ϕ. Two examples are given:

Case I: $\phi = 0$

$$\epsilon_{max} = \frac{da}{R^2}\left(1 - \frac{1}{n}\right)$$

Case II: $\phi \gg \frac{r}{R}$

$$\epsilon_{max} = \frac{d\phi}{R}\left(1 - \frac{1}{n}\right)$$

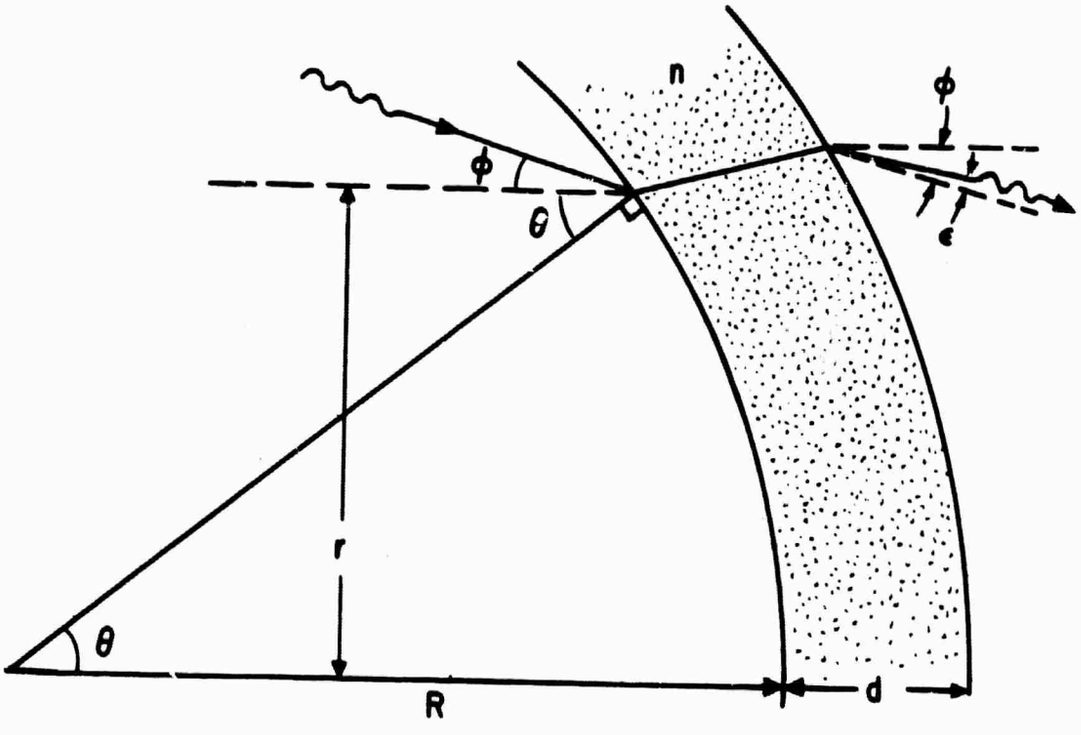

Figure B8. Deflection of Propagation Direction by a Warped Disc

If we choose a fairly typical situation of

$$a = 5 \text{ cm}$$

$$d = 2 \text{ cm}$$

$$R = 10^5 \text{ cm}$$

$$n = 1.5$$

then

$$\epsilon_{max} = \begin{cases} \frac{1}{3} \times 10^{-9} \text{ for Case I} \\ \frac{2}{3} \phi \times 10^{-5} \text{ for Case II} \end{cases}$$

If ϕ is of the order of 10^{-1} radians or less, the increase in beam divergence caused by transmission through a warped disc is small compared to the diffraction effect of $\sim\lambda/2a = 10^{-5}$. Thus, for example, we may construct a multiple disc amplifier using the active mirror configuration with a negligible change in beam divergence even though the discs exhibit some thermal warpage.

OPTICAL THICKNESS

1. Introduction

The 6"D 2% Nd EK ND-11 disc was refinished so one face was flat to $\lambda/10$ and the other face was hand figured to produce less than $\lambda/4$ fringe of etalon interference for $\lambda = 0.63\mu$. This refinishing was performed after the previously reported experiments on thermally induced changes in optical thickness[B1]. The improved optical finish makes it easier to observe small changes in the interference pattern produced by multiple reflections between the front and back face of an illuminated disc. Therefore additional experiments were conducted in an attempt to observe the thermally induced change in optical thickness and variations in this change across the face of the disc which might arise from non-uniform illumination by the pumping light. The experimental procedure was essentially the same as that described previously.[B1] With the aid of auxiliary optics, a 6"D collimated uniphase beam from a Perkin-Elmer Model 5200 CW He-Ne gas laser operating at 0.6328 μ illuminated the laser disc. The disc was tipped slightly so that the interferometric pattern obtained with the gas laser beam could be reflected onto a viewing screen. Photographs were taken of the interference pattern displayed on the viewing screen before and at various time intervals after the pumping lamps were fired.

2. Review of the Theory

If an optical medium of length L under no stress and within an isothermal environment has an optical path length L_{opt} given by

$$L_{opt} = nL$$

where n = refractive index, then the change in L_{opt} caused by a temperature rise $\overline{\Delta T}$ (averaged over the thickness) is given by:(B1)

$$\Delta L_{opt} = L \left(\beta n + \frac{\partial n}{\partial T} \right) \overline{\Delta T}$$

where β = linear expansion coefficient.

The fringe shift f observed in the interference pattern due to $\overline{\Delta T}$ is given by:

$$f = \frac{\Delta L_{opt}}{\lambda / 2} = \frac{2L}{\lambda} \left(\beta n + \frac{\partial n}{\partial T} \right) \overline{\Delta T} \qquad (B6)$$

For neodymium-doped silicate glass

$$\beta = 1.08 \times 10^{-5} / {}^{o}C$$

The temperature dependence of the index of refraction of the glass observed in this experiment is similar(B2) to that of EK No. 11 glass. From the published data(B3) on this glass we infer that:

1) $\frac{\partial n}{\partial T} \sim 0.68 \times 10^{-6} / {}^{o}C$ at $\lambda = 0.63\mu$

2) $\frac{\partial n}{\partial T} < 0.68 \times 10^{-6} / {}^{o}C$ at $\lambda = 1.06\mu$

Since $n \sim 1.6$ at these two wavelengths, we see that the $\frac{\partial n}{\partial T}$ term in Eq. B6 is negligible.

3. Comparison of Theory and Experiment

Since we have calculated(B1) that a pump energy of ~27,000 joule produces an average temperature rise of $0.3^{o}C$ we expect that a pump energy of 30,000 joules will yield $\overline{\Delta T} \sim 0.3^{o}C$. We can now predict that f~0.4 fringe for 30,000 joules of stored pump energy.

Figure B9 shows the series of photographs taken for a pump input energy of 30,000 joules. Comparing the picture taken 10 minutes before the pumping lamps were triggered with the picture taken ~1 sec. after the pumping pulse, we see that there appears to be a shift of ~1/2 fringe in good agreement with our predictions. It is very difficult to estimate a fringe shift of less than unity by simply observing these photographs. The contrast and shading depends upon the photographic exposure, film type, and development time. This fact precludes a direct visual estimate of the degree of uniformity of heating across the face. However we can estimate the uniformity indirectly.

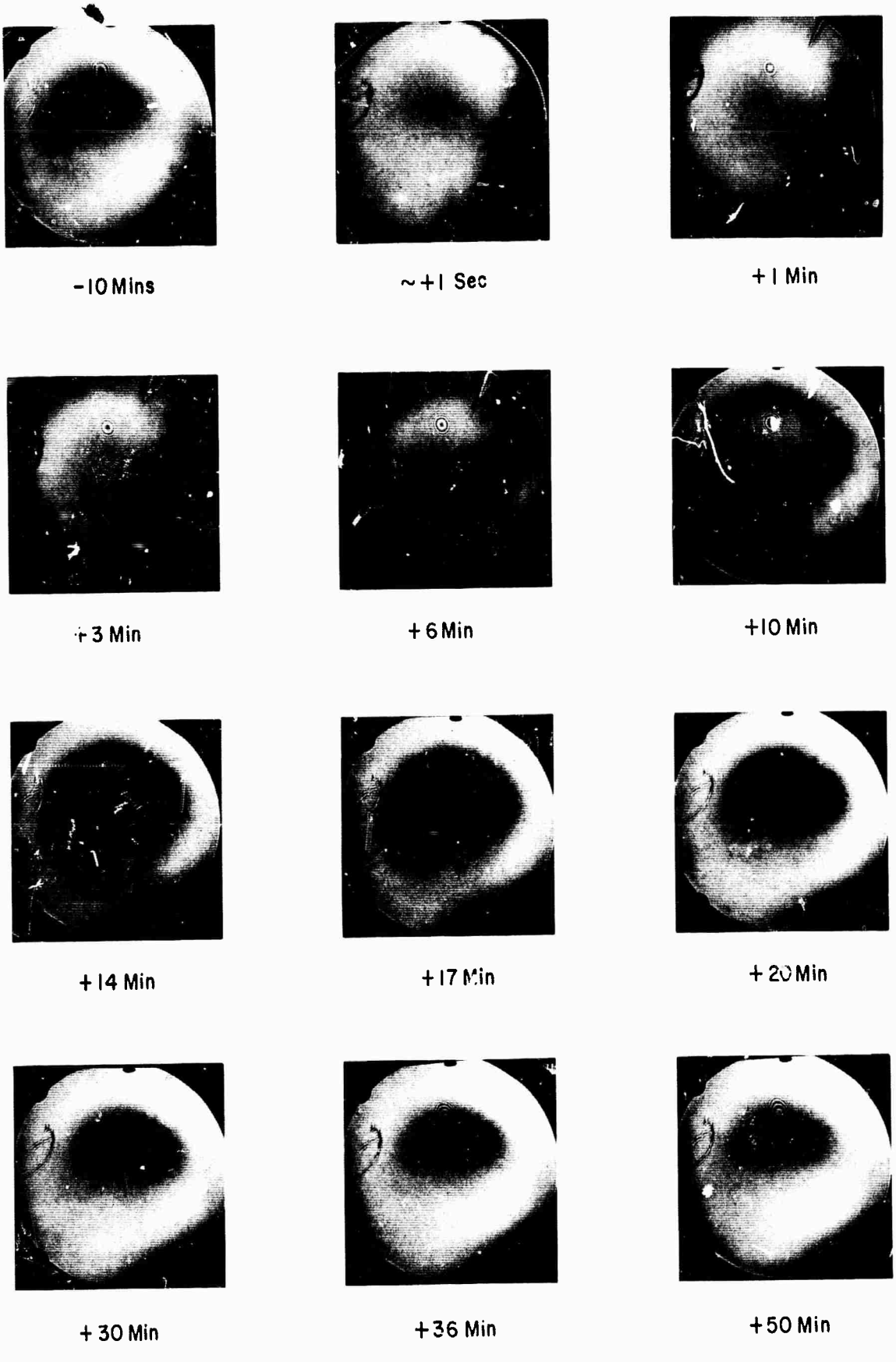

Figure B9. Interferograms as a Function of Time for 6"D Laser Disc and 30,000 Joules of Stored Pump Energy

We have taken another set of photographs of a "cold" (unpumped) disc where each picture differs only slightly in the angle of incidence for the gas laser beam. This change in angle caused the disc to present a slightly different optical thickness for production of the interferogram. Through this technique, we can photograph the interferogram for any arbitrary optical thickness (within generous limits). The important point is that since the disc is "cold" (in equilibrium with the room temperature), the disc has a uniform temperature. Therefore these interferograms necessarily correspond to different uniform changes in optical thickness across the disc face. Now we can try and match up photographs taken by tipping a cold disc with those obtained by heating a disc with a pumping pulse. If we get a perfect match, the heating in the pumped disc must be uniform. Figure B10 shows such a comparison. We have masked off the edge where light leaks around the disc and also a small portion of the left side where the disc is chipped and we do not expect uniform heating. The two left interferograms of Eq. B10 show a comparison of the interferogram taken ~1 sec after a pump energy of 30,000 joules with an interferogram obtained after a small tipping of the cold disc. The two right interferograms of Fig. B10 are similar in that the match is made to the interferogram taken one minute after the pumping pulse. The excellent match in both cases indicates excellent uniformity of heating.

If a discrepancy in this match corresponding to 1/4 fringe occurred, it would probably be discernible. Failure to observe such a discrepancy leads us to conclude that the optical thickness remains uniform within $\lambda/8$ ($\lambda = 0.63\mu$) across the aperture of the disc. It should be noted that our experimental procedure would not detect fluctuations in uniformity occurring within the duration of the pumping pulse. We have examined only the integrated effect.

4. Estimate of Beam Degradation Arising From Thermally Induced Thickness Fluctuations Across the Aperture

We have concluded that the variation in disc thickness is $\lesssim \lambda/8$ at $0.63\,\mu$ or $0.074\,\lambda$ at $1.06\,\mu$. For example, assume that variations of this magnitude actually occur caused by integrated output of one of the flash lamps exceeding the average. Then we may have a surface profile of the disc which resembles that depicted in Fig. B11. The distortion corresponds to a maximum radius of curvature R given by

$$R = \frac{r^2}{2m}$$

where m = maximum out-of-plane displacement which we claim to be less than $0.074\,\lambda$. The symbol r is defined in Fig. B12. Now the maximum angle θ between the distorted surface tangent and the reference surface of the undistorted disc is given by (see Fig. B12).

$$\theta = \frac{a}{R}$$

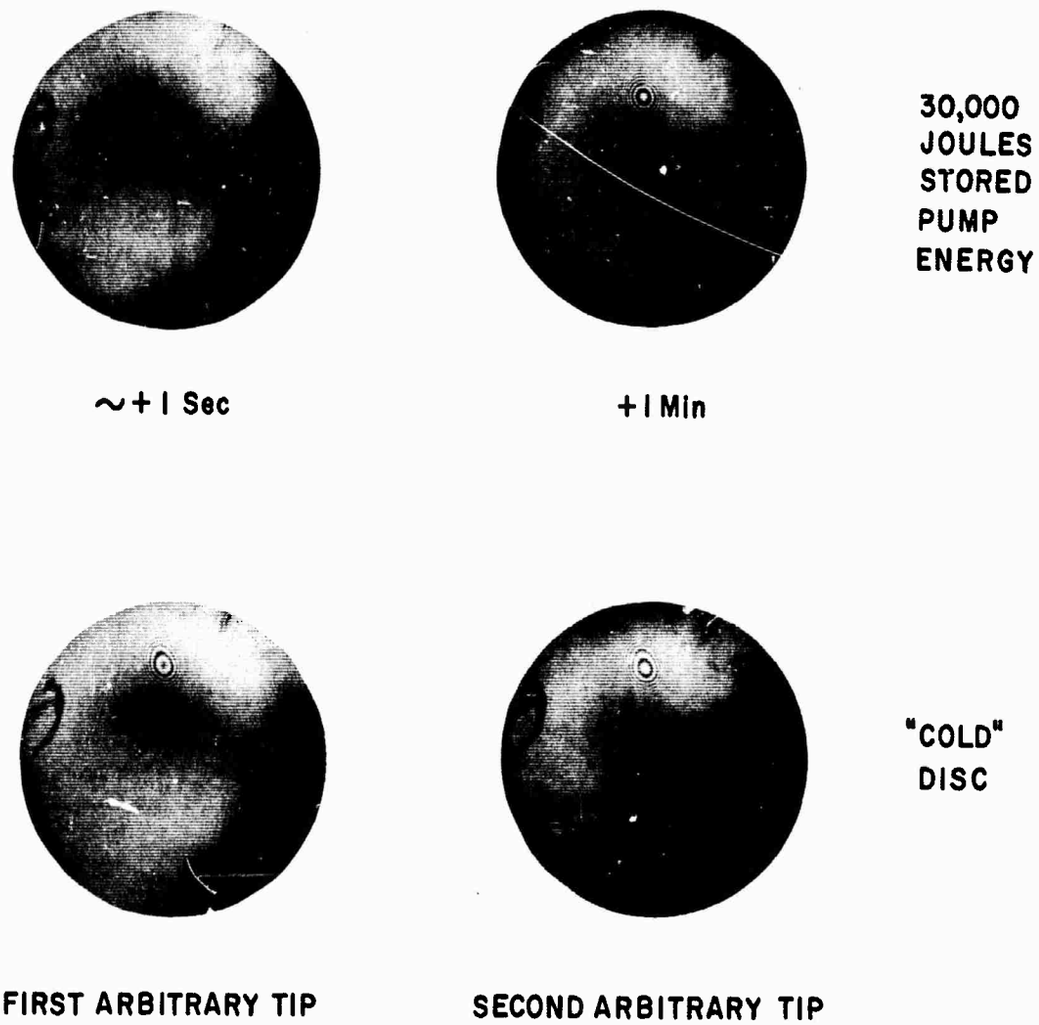

Figure B10. Comparison of Interferograms for Optically Pumped Disc and Tipped Cold Disc

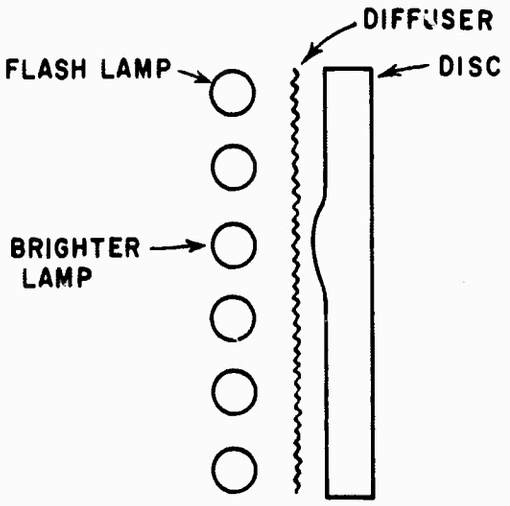

Figure B11. Schematic of Thickness Variation Arising from Non-Uniform Pumping

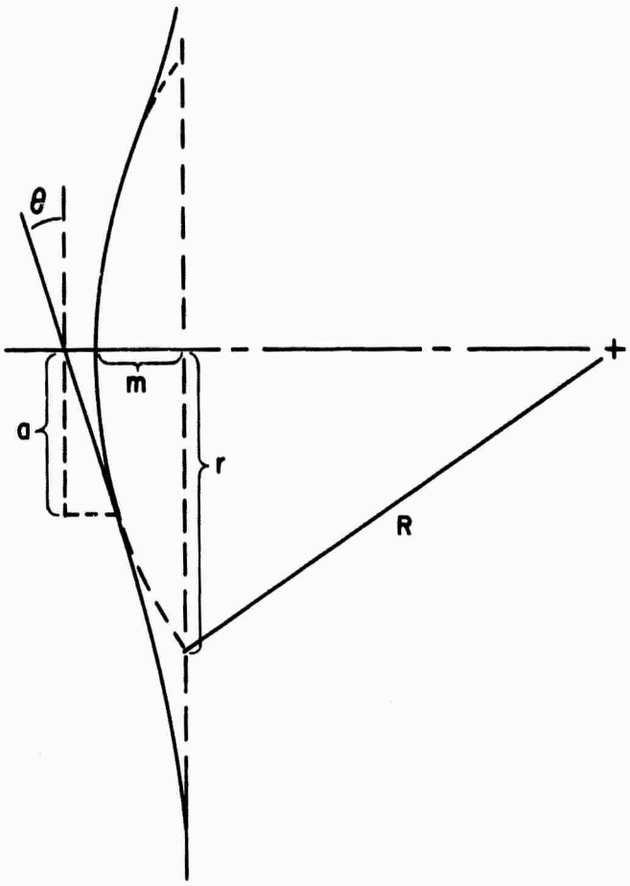

Figure B12. Approximation to Surface Profile

In the following analysis we calculated the amount of beam degradation on a parallel incident beam caused by this distorted surface. From Fig. B13 we see that the beam deviation is given by $\epsilon = \theta(n-1)$. Considering the effect of the diffuser, it seems unlikely that "r" and/or "a" would be less than 1-cm. To get an idea of the upper limit on the beam distortion let us assume $a = r/2 = 1$ cm and $n = 1.6$. Then

$$\epsilon = \frac{m}{r}(n-1)$$

$$\epsilon \sim 5 \times 10^{-6} \text{ radians}$$

This is the order of magnitude of θ_D, the diffraction limited beam angle.

This type of analysis gives us a feeling for the optical finish required for a disc in a traveling wave amplifier. For example, if the optical thickness could be described by

$$d = d_o + m \sin\left(\frac{\pi x}{2p}\right)$$

where m is the maximum out-of-plane displacement and 4p is the oscillation period then, we find that

$$\epsilon = \frac{(n-1)\pi m}{2p}$$

If we desire that

$$\epsilon < 10^{-5}$$

and we let p = 1 cm, n = 1.6, and $\lambda = 1.06 \times 10^{-4}$ cm we find that

$$m < \lambda/10$$

Thus the surfaces of the discs in a traveling wave amplifier should be flat within $\lambda/10$.

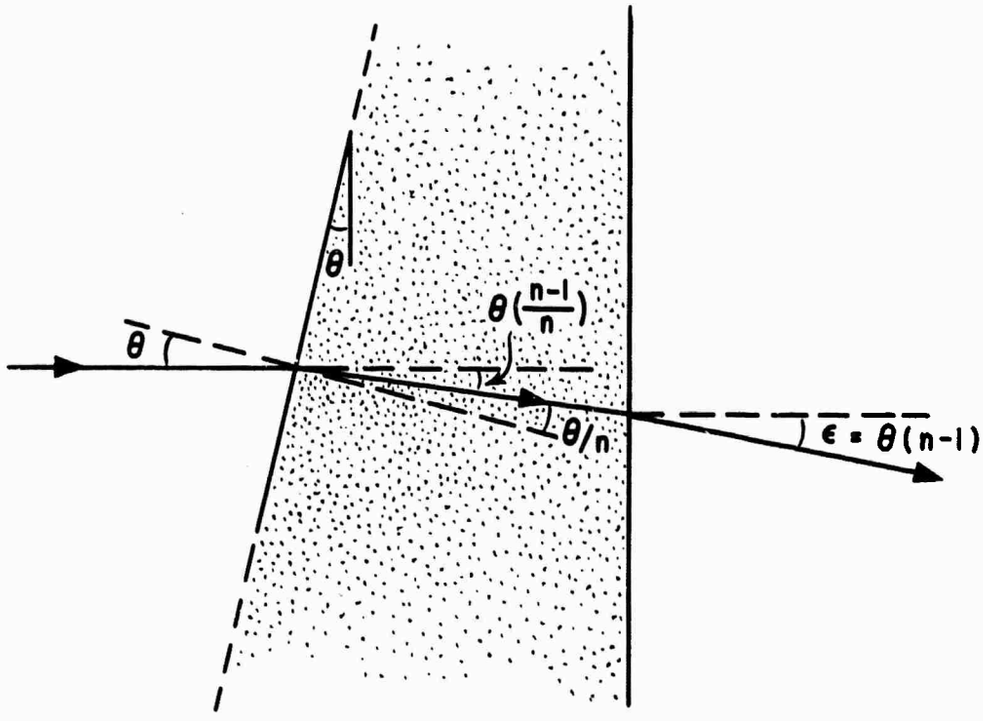

Figure B13. Ray Deviation through Disc with Non-Parallel Sides and Index of Refraction n

C. AMPLIFIED SPONTANEOUS EMISSION

In order to obtain more information on the effect of certain changes on amplified spontaneous emission (super radiance), additional experiments were conducted. The experimental arrangement was similar to the one reported earlier(B1). The pump light was monitored with a photodiode and the 1.06 μ lateral fluorescence intensity was fed into a RCA-7102 photomultiplier through a 70 Å-wide transmission filter. The light pipe "collimator" combination was changed to that shown in Fig. C1. Three additional changes were made in the experiment:

1. When the 6"D 2% Nd EK ND-11 disc was refinished for better flatness on both faces, two small flat areas, opposite and parallel to each other, of approximately 1/2" width were ground on the cylindrical surface of the disc and polished to an optical smoothness. One of these two flat areas was used as a port for observing lateral fluorescence and thus we avoided the directional integration entailed in observation through a ground glass surface. In addition, a different set of fluorescent rays were observed on reflection off the opposite flat surface.

2. In series with each of the six flash lamps, 0.6 ohm resistors were used in the former experiments. With these resistors the circuit was critically damped, and no ringing was observed when the pumping pulse was quickly terminated by the crowbar circuit described previously. For the refined experiments, these six resistors were removed and some ringing was observed. However the light output from the lamps increased by ~70 percent and greater population inversion was obtained.

3. The cylindrical surface could be blackened to minimize reflection, and observations through one flat area were made with a) no blackening at all, b) the entire cylindrical surface blackened except for the one flat area observation port, and c) only one flat area blackened.

In these refined experiments on amplified spontaneous emission, the lateral fluorescence is observed nearest the pumped face where the inversion is highest and the problem of amplified spontaneous emission is expected to be most severe. With the disc modified as described above, the fluorescence through one of the flat areas was detected and then displayed on an oscilloscope.

With no blackening on the flat polished surfaces, the four percent reflection of the spontaneous fluorescence emission was sufficient to cause lasing action in the lateral direction. Application of a thin film of mineral oil on the flat area opposite the observation port prevented lasing in these refined experiments; the peak of fluorescence intensity was noted but a lifetime measurement was not made. In the earlier experiments lateral lasing was not evident but

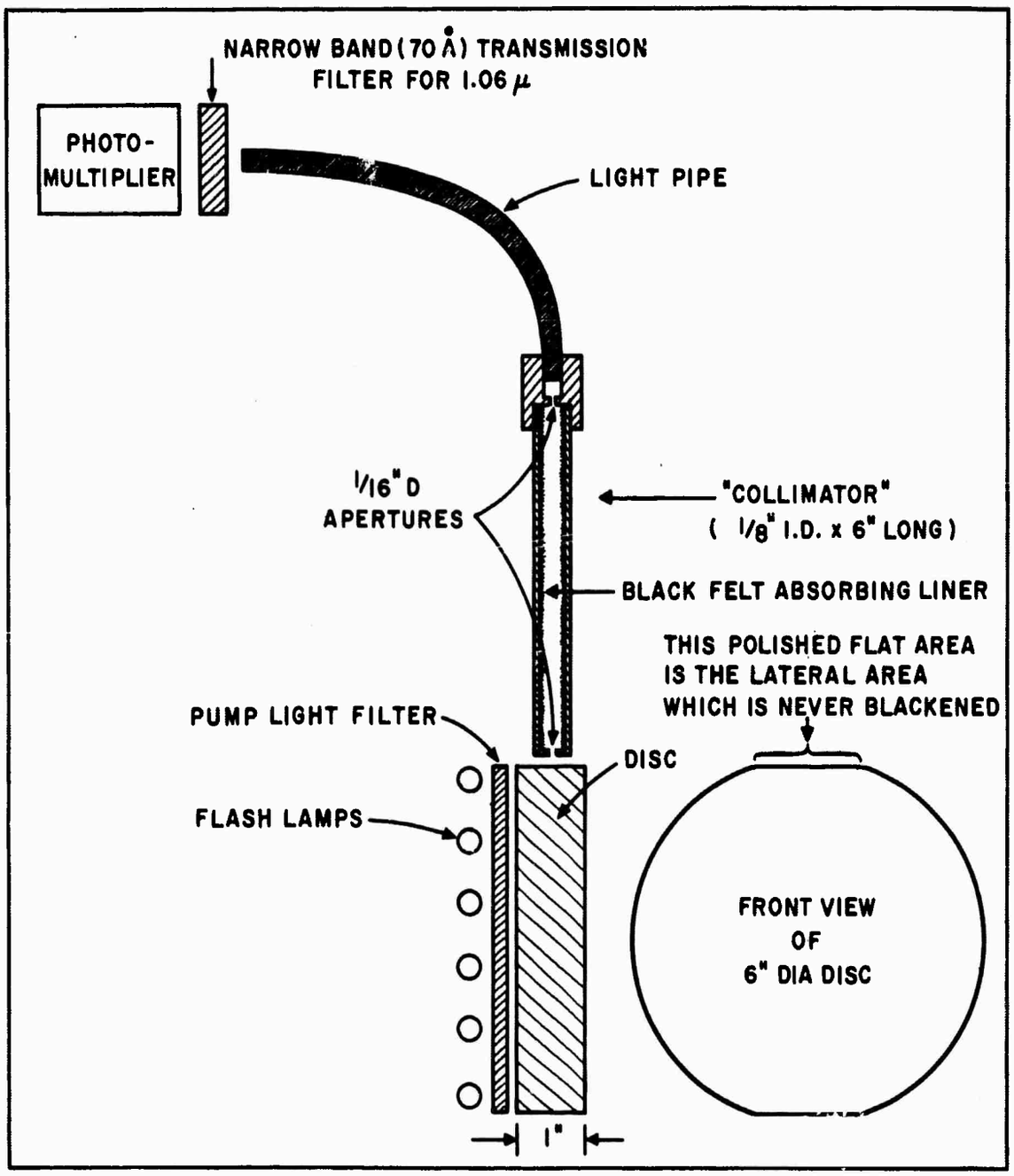

Figure C1. Schematic Diagram of Lateral Fluorescence Experimental Setup

a lifetime shortening of about 33 percent was observed so presumably the lasing condition was being approached. In the same earlier experiments, 40 percent less pumping energy was actually delivered to the disc due to the 0.6 ohm resistors in the lamp circuits discussed above.

In Fig. C2 the upper and lower oscilloscope traces are pumping and fluorescence intensity traces respectively as a function of time for stored pump energies of 6000, 9375 and 13,500 joules. After 600 μsecs, a) the crowbar circuit was fired to terminate pumping, and b) the fluorescence intensity traces were initiated. For these oscilloscope traces, the entire cylindrical surface was blackened, except for one flat area observation port, with Kodak No. 4 Dull Black Lacquer. The fluorescence intensity decreased by a factor of ~2.2 over the case where the oil coated the flat area opposite the observation port. The fluorescence lifetime is measured by taking the slope of the fluorescence intensity at a time of 100 μsec after firing the crowbar. With 6000 and 13,500 joules of stored energy the measured lifetimes were 360 and 330 μsec respectively which gives an eight percent shortening of the lifetime. This shortening is comparable to the experimental uncertainty.

With the blackening removed by using acetone, the fluorescent intensity did not increase as initially expected by a factor of 2.2 but only ~1.5. Presumably the discrepancy is due to the fact that it was not possible to remove all of the blackening from the ground surface by this technique. Still there is ~11 percent lifetime shortening for 6000 joules of stored energy while at 13,500 joules there is lateral lasing again. With only the flat area opposite the observation port blackened, the lifetime shortening was reduced to an acceptable level. All of these fluorescence lifetime measurements are presented in Table C-I.

For the 6"D 2% Nd EKND-11 disc, it can be concluded that amplified spontaneous emission is not a serious problem provided the cylindrical surface can be blackened in order to prevent the fluorescent rays from making multiple passes through the active medium. It should be noted that Kodak No. 4 Dull Black Lacquer does not match the refractive index of the glass and therefore there is some reflection at the surface. However, black lacquer which matches the refractive index of glass can be obtained. In addition, more elaborate schemes involving glass cladding doped with 1.06 μ-absorbing ions can also be used.

These data will be useful in evaluating new combinations of doping concentration, fluorescence lifetime and disc geometry.

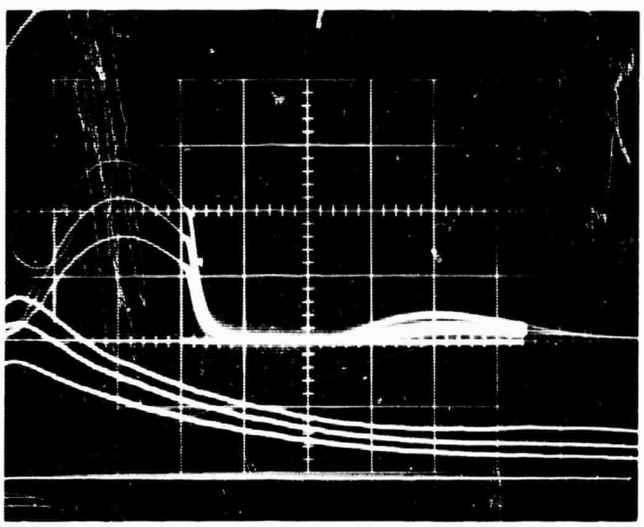

PUMPING INTENSITY
(200 μsec/div.)

LATERAL FLUORESCENCE
INTENSITY WITH TIME
DELAY OF 600 μsec.
(100 μsec/div.)

PUMP STORED ENERGY OF
6000, 9375 AND 13,500 joules

Figure C2. Pumping and Lateral Fluorescence Intensities as a Function of Time and Pumping Level

TABLE C-I - FLUORESCENCE LIFETIME OF PUMPED DISC

Experiment		Fluorescence Lifetime 6000 J	Fluorescence Lifetime 13,500 J	Maximum Lifetime Shortening Beyond 360 μsec
Former Results		360 μsec	240 μsec	33%
New Results	No Blackening on Polished Flats	Lateral Lasing	Lateral Lasing	Very Large
	Blackened Entire Cylindrical Surface Except Observation Port	360 μsec	330 μsec	8%
	Blackening Removed	320 μsec	Lasing	Very Large
	Blackened Only the Flat Area Opposite the Observation Port	350 μsec	310 μsec	14%

D. PUMP ASSEMBLY

PUMPING POWER

To facilitate the experimental work and permit the use of the newly developed laser glasses, a pump assembly to accommodate discs three inches in diameter was designed and assembled.

The pump assembly, shown in Fig. D1, consists of a bank of six FX-42 xenon flash lamps located 2 cm from the back face of the laser disc. Interposed between the lamps and the laser disc is a 1-cm thick Pyrex filter cell containing a solution consisting of a 1/10 percent concentration of potassium chromate in water. The transmission characteristic of the filter is shown in Fig. D2. The purpose of this filter is to prevent the useless ultraviolet and infrared radiation of the xenon lamp discharge from reaching the laser disc.

A series of measurements were carried out to determine the optical efficiency of a three inch pump configuration. This consisted of placing a ballistic thermopile type of calorimeter against the face of the laser disc and observing the energy transmitted through the disc. The laser disc was then removed and replaced with a non-absorbing glass plate having a multiple layer dielectric mirror similar to that on the pumped face of the disc. The measured results are shown in Fig. D3. The difference between the two energy measurements is the energy absorbed in the laser disc. The results of these measurements are shown in Fig. D4.

The 1-cm thick laser disc was fabricated from American Optical MG-702 7% Nd glass. With the maximum lamp input energy of 9000 joules (1500 joules per lamp) the energy absorbed in the disc was 6.5 joules per square cm of disc area. The shape of the pump pulse was nearly rectangular with a duration of one millisecond. This indicates a power absorption in the neodymium pumping bands falling between 5000 and 10,000 Å of 6.5×10^3 watts/cm^2.

From Fig. D4, it can be seen that the pumping rate falls off from a linear function at the higher lamp loadings because of the shift in the radiation spectrum to the ultraviolet.

OPTICAL COUPLING EFFICIENCY

The theoretical maximum optical coupling provides a radiation density incident on the face of the disc equal to that radiated from the lamp surface. This coupling can be realized by completely filling the area behind the disc with an opaque radiating lamp surface. In practice this cannot be done because of the physical limitations imposed by the lamp mountings and the finite wall thickness of the lamps.

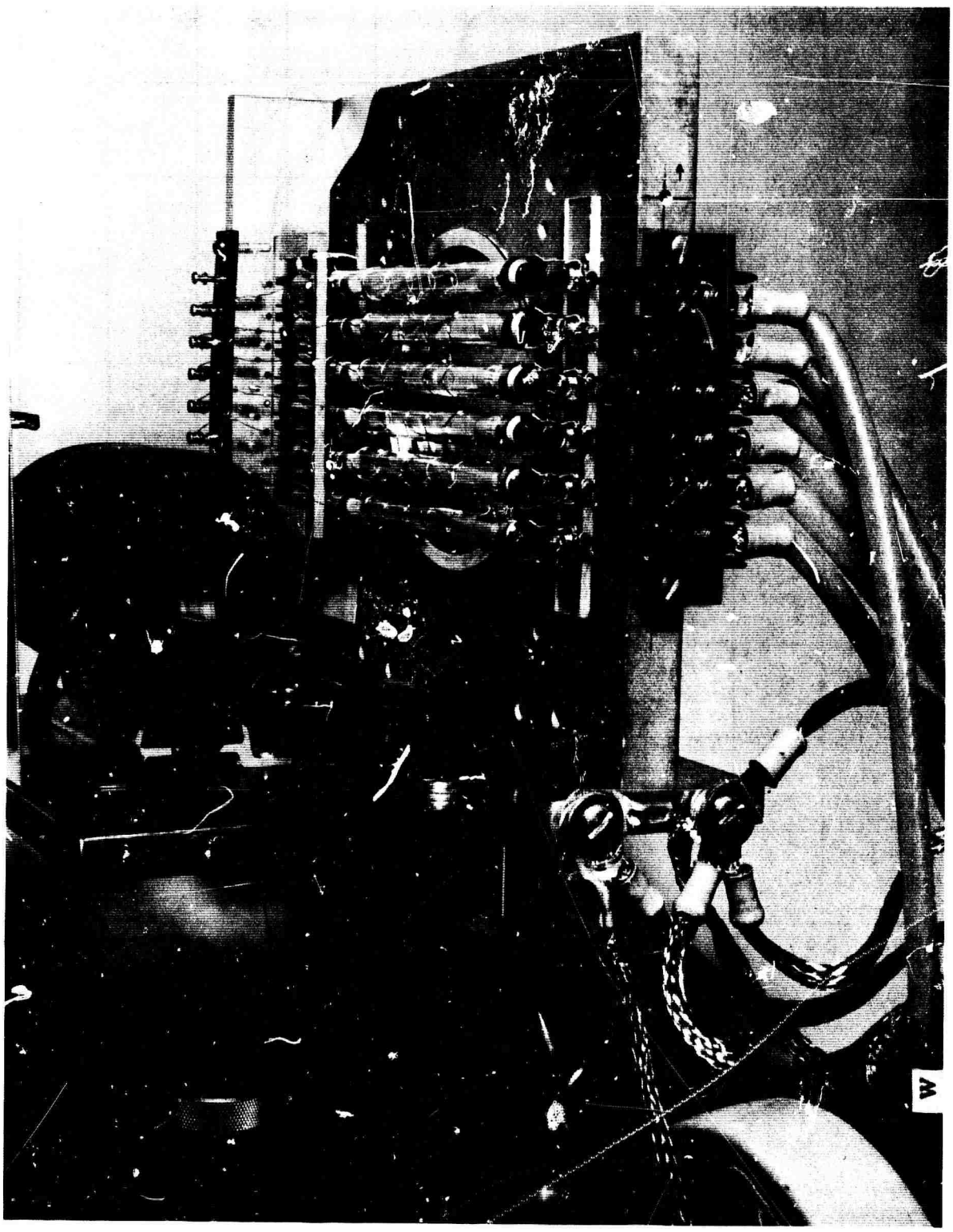

Figure D1. Rear View of 3-Inch Disc Assembly with Diffuse Reflector Removed

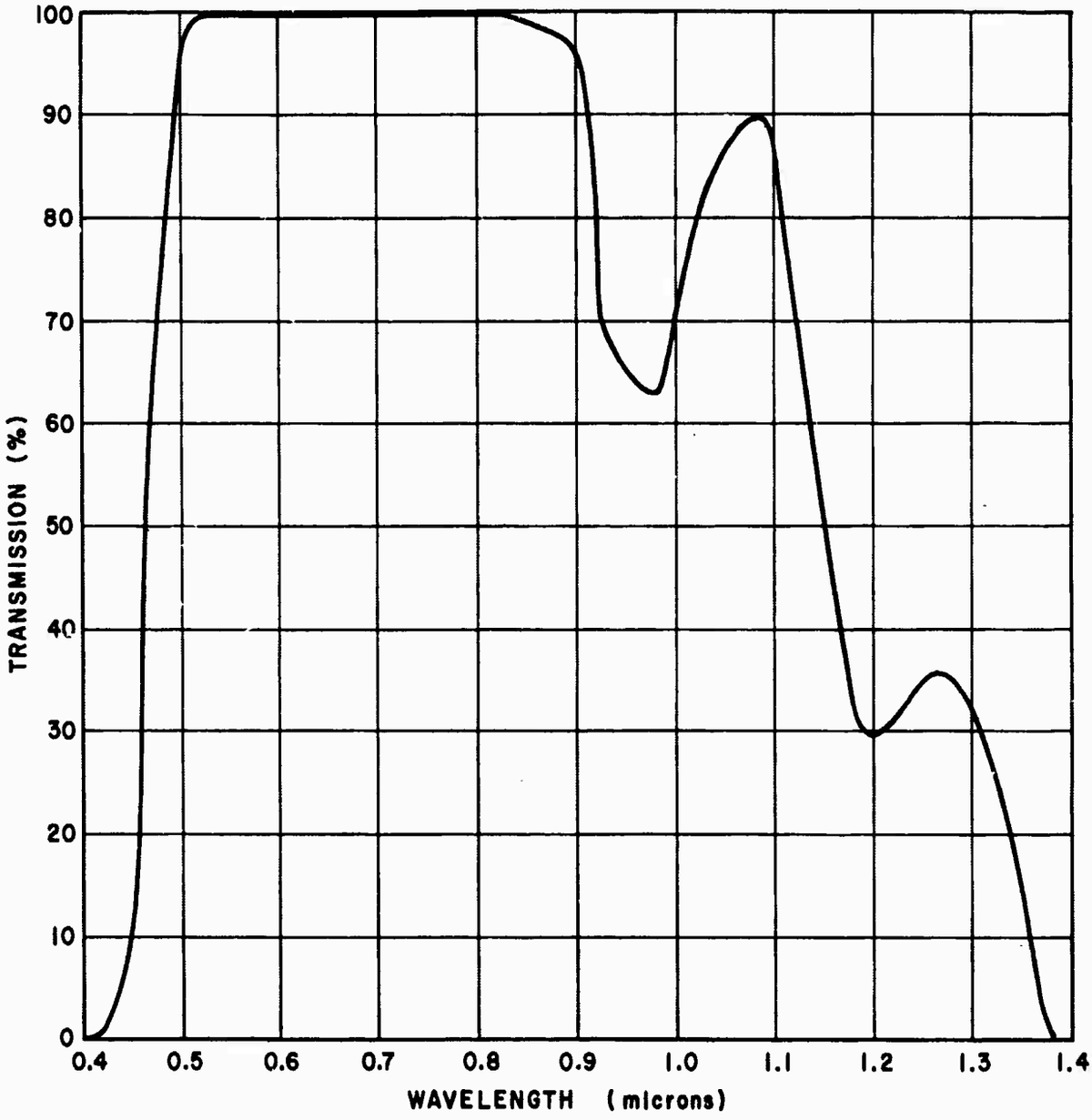

Figure D2. Transmission of Potassium Chromate Water Filter

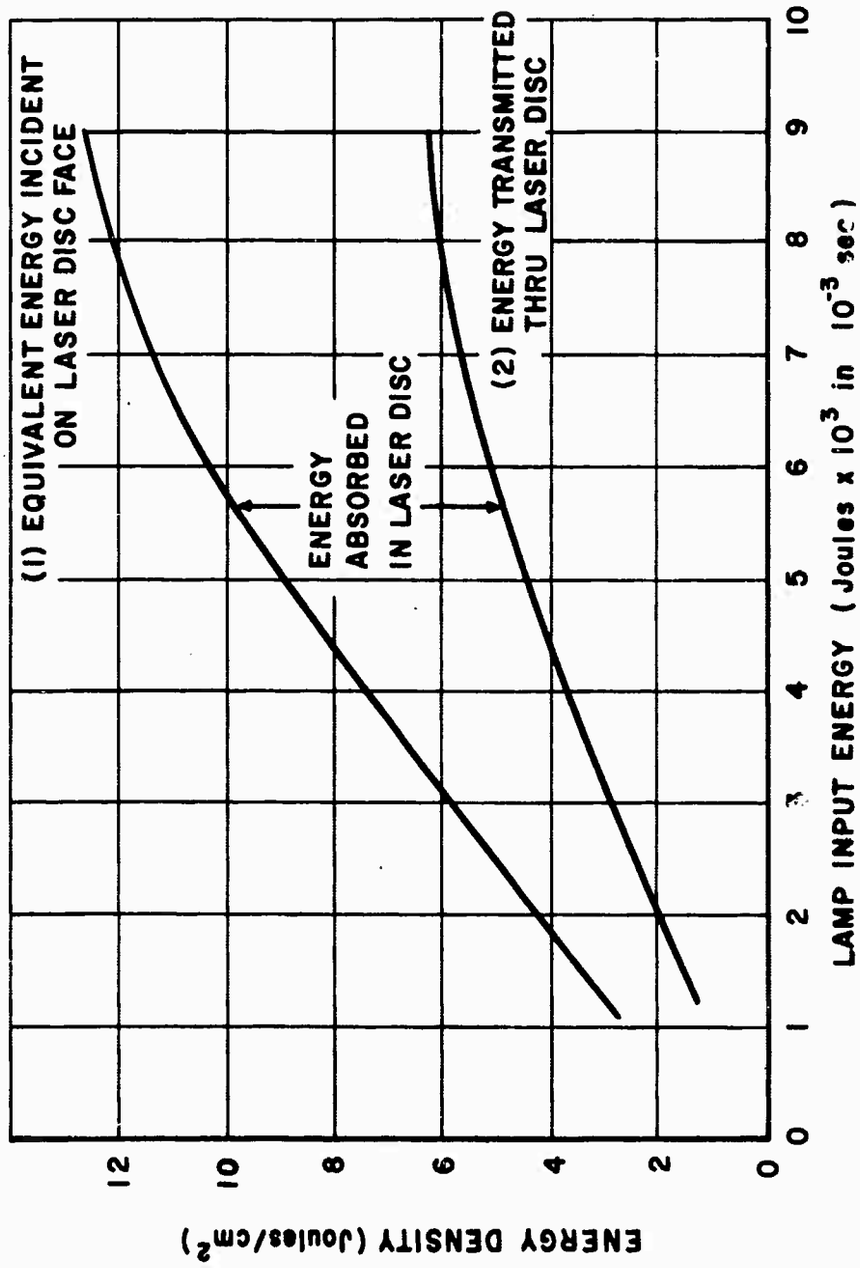

Figure D3. Energy Density Measurements

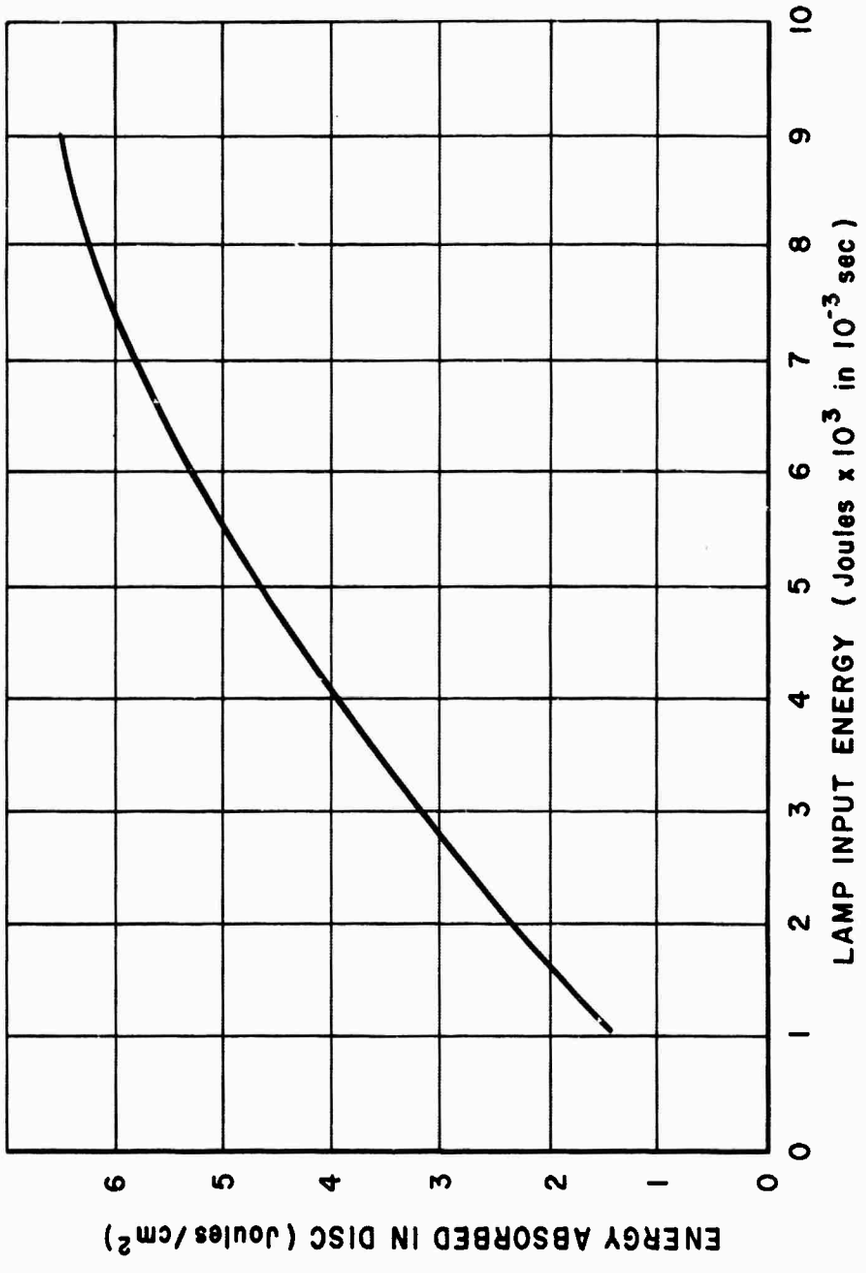

Figure D4. Energy Absorbed in Laser Disc

In the three inch pump assembly, the laser disc with a diameter of 75 mm faces six lamps of 7 mm bore diameter. Thus the projected area of the lamps covers only 56 percent of the area of the array of lamps. To fill in the regions between the lamps we have placed a diffuse reflector made of a high-alumina ceramic having a reflectivity of 98 percent behind the lamps. The effect of this reflector was determined by measuring the radiation density at the disc location with the reflector in place and with the reflector removed. The reflector was found to increase the radiation density at the disc face by 65 percent at low lamp loading and 50 percent at high lamp loading. This would indicate that at low lamp loading the lamp plasma was not completely opaque permitting more of the reflected radiation to reach the disc than at high lamp loading.

From this it can be seen that there remains a factor of about 1/5 at high lamp loading by which the pumping radiation density could be increased either by closer lamp spacing or improved reflector design.

PUMP REFLECTION LOSS BY DIELECTRIC MIRROR

A calorimetric measurement similar to that described earlier was carried out to determine the loss of pump radiation resulting from the multiple layer dielectric mirror on the pumped face of the disc. Using a transparent plate of glass with the same type of multiple layer dielectric mirror as that applied to the disc, radiation density measurements were made with and without the plate in place. The dielectric mirror was found to be ~80 percent transmitting to the radiation incident on the disc in the wavelength region falling between 5000 and 10,000 Å. From this data, we expect that the reduction in the maximum inversion is ~20 percent although the exact figure depends upon a detailed matching of the mirror transmission and active medium absorption spectrum. An analysis of the inversion distribution, with and without the dielectric mirror, confirms that 20 percent is the approximate reduction in population inversion due to the multiple layer dielectric mirror on the pumped face of the disc.

DIELECTRIC MIRROR DURABILITY

Originally the pump assembly utilized a Corning 0-52 glass which starts cutting off the ultraviolet at about 3800 Å. Even with this filter we observed some damage to the dielectric mirror at the higher lamp powers. The filter was replaced with a potassium chromate filter which starts to cut off at about 5000 Å. After operating the pump assembly for over 100 flashes there was no damage to the dielectric mirror or the laser disc that could be attributed to pump radiation.

E. DISTORTION EFFECTS IN A PLANE-MIRROR FABRY-PEROT RESONATOR

In a plane-mirror Fabry-Perot resonator a deformation corresponding to either a small tilt or a slight curvature of the mirrors will produce mode conversion effects. The following mode conversion analysis is very preliminary with some simplifying assumptions. It is assumed that a monochromatic plane wave initially exists within the resonator and the validity of this assumption in a laser resonator is certainly an open question. It will be assumed that the Fresnel number, $a^2/\lambda L$, of the resonator is very large ($\sim 10^4$ in our cases) and with this assumption diffraction losses can be neglected and the plane wave description seems more plausible. Scattering losses are also neglected.

The mode conversion analysis is based on the concept that the wave form of the laser oscillation mode is preserved through the reflection of a wave front from a surface slightly incompatible with it by the generation of another wave which just compensates for the phase mismatch. By characterizing an undistorted ideally reflected wave w_o, the actual reflected wave w_r, and the compensating wave w_c, we can represent this assumption by:

$$w_r + w_c = w_o \tag{E1}$$

In order to proceed further, we require w_o.

In the case of large Fresnel number plane parallel mirrors perpendicular to the x axis, the incident modal wave front of interest may be given by

$$w_i = A_i e^{i(px-\omega t)} \tag{E2}$$

and the undistorted reflected wave is

$$w_o = A_o e^{-i(px+\phi+\omega t)} \tag{E3}$$

where A is the wave amplitude, $p = 2\pi/\lambda$, λ is the wavelength of the modal radiation, and ϕ_o allows for a phase shift on reflection. In this case of plane parallel mirrors, the reflecting surface is compatible with the modal wave front so that $w_r = w_o$ and $w_c = 0$.

If, however, the mirrors are not quite parallel but make a small angle 2δ with each other, it seems plausible to assume that the lowest loss modal wave front lies in a plane bisecting the angle of divergence. If we place the x axis perpendicular to this wave front then we have the situation depicted in Fig. E1 where we let the mirrors lie between $y = \pm a$. Once again we represent the modal wave with a plane wave traveling to the right so that

$$w_i = A_i e^{i(px-\omega t)} \tag{E4}$$

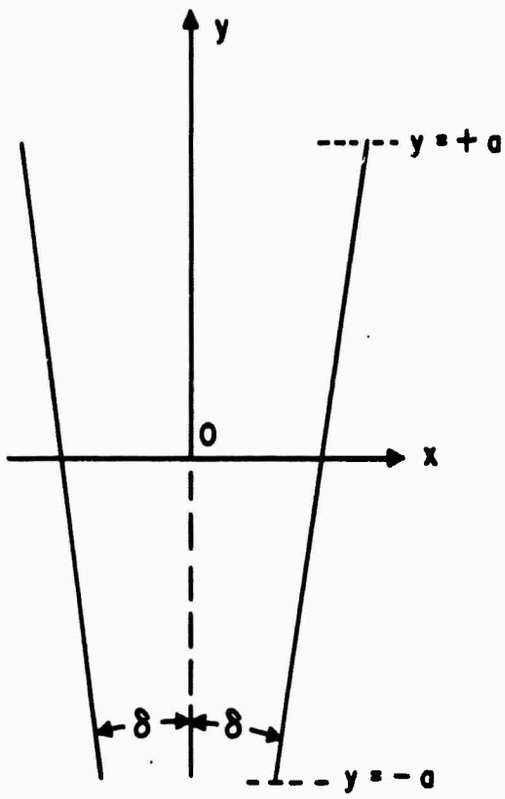

Figure E1. Fabry-Perot Resonator with Slightly Tilted Plane Mirrors

The desired reflected wave is again

$$w_o = A_o e^{-i(px+\phi_o+\omega t)} \tag{E5}$$

The actual reflected wave is

$$w_r = A_o e^{-i(p'x-q'y+\phi+\omega t)} \tag{E6}$$

From geometric optics we find that

$$\frac{q'}{p'} = \tan 2\delta \tag{E7}$$

In order that $(q')^2 + (p')^2 = p^2$ we find that

$$\begin{aligned} q' &= p \sin 2\delta \sim 2\delta p \quad \text{if} \quad \delta \ll 1 \\ p' &= p \cos 2\delta \sim p \qquad \text{if } \delta \ll 1 \end{aligned} \tag{E8}$$

Now we may use Eq. E8 to rewrite Eq. E6 as follows:

$$w_r = A_o e^{-i(px-2\delta py+\phi+\omega t)} \tag{E9}$$

We note that, to first order in δ, the effect of the phase mismatch between the mirror surface and the incident modal wave front is simply to add a phase shift of $2\delta py + (\phi_o-\phi)$ to w_o. Recalling that $p = 2\pi/\lambda$ we note that

$$2\delta py = 2\pi\left(\frac{2\delta y}{\lambda}\right) \tag{E10}$$

The factor $2\delta y$ just represents the extra path length that the modal wave must travel because of the mirror tilt if the pivot line of the tilt is about the mirror center ($y = 0$). Thus $2\delta py$ represents the extra phase shift introduced by tilting the mirror about its center while $\phi_o - \phi$ accounts for the possibility of tilting the mirror about some other line with coordinate $y \neq 0$.

The compensating wave may now be calculated from Eqs. E1, E5, and E9:

$$w_c = w_o \left(1 - e^{i\left[2\delta py+(\phi_c-\phi)\right]}\right) \tag{E11}$$

If we let

$$\theta \equiv \phi_o - \phi \tag{E12}$$

then

$$w_c = w_o \left(1 - e^{i(2\delta py+\theta)}\right) \tag{E13}$$

Assuming the extra phase shift introduced by the tilt deformation is small, we may expand the exponential in Eq. E13. Then:

$$w_c = -i\, w_o\, (2\delta py + \theta) \tag{E14}$$

The -i factor shows that w_c is in phase quadrature with w_o which is what we expect since, to first order in δ the only effect of the tilted mirror is the introduction of a phase shift. A correction wave in phase quadrature with the reflected wave compensates for the phase error with negligible change in amplitude. Because w_c is in phase quadrature with w_o and w_r, we may calculate its relative energy without regard to w_o and w_r. The energy carried by w_c must be supplied by the laser medium in order to preserve the mode and thus this energy, when normalized to the energy of the undiminished wave w_o, represents the fractional power loss P caused by tilting the mirror. Thus

$$P = \frac{\int w_c^* \, w_c \, dS}{\int w_o^* \, w_o \, dS} \tag{E15}$$

where the integral is over the cross-sectional area of the cavity, S. Let us further assume that

$$\left.\begin{aligned} A_o(y) &= 1 \quad \text{for} \quad -a \leq y \leq a \\ A_o(y) &= 0 \quad \text{for} \quad (y) > a \end{aligned}\right\} \tag{E16}$$

i.e., the modal wave is of constant amplitude which is probably fairly realistic for our large Fresnel number ($\sim 10^4$) system. Then noting that $w_o^* w_o = 1$ and substituting Eq. E14 into Eq. E15 yields:

$$P_{tilt} = \frac{\int_{-a}^{+a} \int_{-a}^{+a} (2\delta py + \theta)^2 \, dy \, dz}{\int_{-a}^{+a} \int_{-a}^{+a} dy \, dz} = \frac{1}{3} (2\delta pa)^2 + \theta^2 \tag{E17}$$

We note that the power loss depends upon θ which is related to the pivot axis for the tilt deformation or alternatively on the value of y for which there is no phase mismatch and $w_c = 0$. We expect the modal wave of interest to satisfy the condition that P is a minimum. Hence we determine θ by requiring that

$$\frac{\partial P}{\partial \theta} = 0 \tag{E18}$$

For P_{tilt} as given by Eq. E17 the solution to Eq. E18 is trivial ($\theta = 0$) and we see that the loss is minimized by tilting the mirror about its center as is

intuitively obvious. By letting $p = 2\pi/\lambda$ and $\theta = 0$, we may rewrite Eq. E17

$$P_{tilt}\Big|_{min} = \frac{16\pi^2}{3}\left(\frac{a\delta}{\lambda}\right)^2 \qquad \text{(E19)}$$

Eq. E19 gives the fractional power loss introduced by one reflection off the tilted mirror and this result agrees exactly with Kotik and Newstein(E1).

We have described in some detail the derivation of Eq. E17 yielding the loss P_{tilt} introduced by a tilt deformation in order to provide sufficient insight into the problem to allow the generalization of the method that follows. The term $2\delta py$ in the numerator can be defined as ψ, and this is the extra geometric (two-way) phase shift in the reflected wave relative to the phase shift at the center ($y = 0$) of the mirror due to mirror deformation. The other term θ in the numerator is the two-way phase shift at the mirror center relative to an arbitrary phase plane. Thus Eq. E17 can be rewritten

$$P = \frac{\int(\psi+\theta)^2\, dS}{\int dS} \qquad \text{(E20)}$$

Eq. E20 gives the first order fractional power loss produced by any mirror deformation such that $|\psi+\theta| << |$. Eq. E18 is still used to give the minimum value of P which is the expected observable.

For a small cylindrical mirror distortion with a radius of curvature R, the displacement from the plane is approximately given by $\Delta x = y^2/2R$. Then

$$\psi = 2(2\pi)\frac{\Delta x}{\lambda} = \frac{2\pi y^2}{R\lambda} \qquad \text{(E21)}$$

Then substitution into Eq. E20 yields

$$P = \frac{\int\left(\frac{2\pi y^2}{R\lambda}+\theta\right)^2 dS}{\int dS} = \frac{1}{5}\left(\frac{2\pi}{R\lambda}\right)^2 a^4 + \frac{2}{3}\left(\frac{2\pi}{R\lambda}\right)\theta a^2 + \theta^2 \qquad \text{(E22)}$$

where 2a = total width of the cylindrical surface in the y-direction. Substitution of Eq. E22 into Eq. E18 determines θ:

$$\theta = -\frac{1}{3}\left(\frac{2\pi}{R\lambda}\right)a^2 \qquad \text{(E23)}$$

Hence

$$P_{cylindrical}\Big|_{min} = \frac{64\pi^2}{45}\left(\frac{a^2}{2R\lambda}\right)^2 \qquad \text{(E24)}$$

which agrees exactly with the results of Kotik and Newstein[E1] but is far simpler to derive.

For a small spherical mirror deformation with a radius of curvature R, the out-of-plane displacement $\Delta x = r^2/2R$. Then

$$\psi = 2(2\pi)\frac{\Delta x}{\lambda} = \frac{2\pi r^2}{R\lambda} \qquad \text{(E25)}$$

For this calculation we will consider the mirrors to be circular with a radius "a" instead of square with a width 2a as in the previous calculations. Then substitution of Eq. E25 into Eq. E20 yields:

$$\mathbf{P} = \frac{\int_o^a \left(\frac{2\pi r^2}{R\lambda} + \theta\right)^2 rdr}{\int_o^a rdr} = \frac{1}{3}\left(\frac{2\pi}{\lambda R}\right)^2 a^4 + \left(\frac{2\pi}{\lambda R}\right)\theta a^2 + \theta^2 \qquad \text{(E26)}$$

Substitution of Eq. E26 into Eq. E18 determines θ:

$$\theta = -\frac{1}{2}\left(\frac{2\pi}{\lambda R}\right) a^2 \qquad \text{(E27)}$$

Hence

$$P_{spherical}\Big|_{min} = \frac{4\pi^2}{3}\left(\frac{a^2}{2\lambda R}\right)^2 \qquad \text{(E28)}$$

If we let K be the maximum out-of-plane displacement in wavelengths of the deformed mirror then we may summarize our results in Table E-I. In the last column of the Table we show the values of K which will yield an additional power loss L_a per reflection of 10^{-2}.

TABLE E-I

ADDITIONAL POWER LOSS DUE TO MIRROR DEFORMATION

Type of Mirror Deformation	Definition of K in Wavelengths	Additional Power Loss L_a per Reflection	Value of K for $L_a = 10^{-2}$
Tilted	$\frac{a\delta}{\lambda}$	$\frac{16\pi^2}{3} K^2$	1.4×10^{-2}
Cylindrical Curvature	$\frac{a^2}{2\lambda R}$	$\frac{64\pi^2}{45} K^2$	2.7×10^{-2}
Spherical Curvature	$\frac{a^2}{2\lambda R}$	$\frac{4\pi^2}{3} K^2$	2.8×10^{-2}

F. OSCILLATOR EXPERIMENTS

INTRODUCTION

Operation of the active mirror as a disc laser oscillator was undertaken as a means of evaluating the active mirror configuration. Measurements of threshold vs. cavity loss provide an indication of the gain and inversion level achieved in the pumped disc.

Several active mirror discs fabricated from different Nd doped glasses were studied. Not only did these glasses differ in Nd concentration and lifetime but, unfortunately, the optical quality of the finished discs also differed significantly, often failing to meet our specifications. These variations in optical quality preclude an integrated discussion of the discs since, as we have seen in the preceding Part E, these distortions easily lead to additional cavity losses of several percent per transit. In the following paragraphs, laser threshold experiments using AO MG-702 glass segments are described, and these are followed by some limited experiments using other neodymium-doped glass discs.

AMERICAN OPTICAL MG-702 NEODYMIUM-DOPED GLASS

The most extensive laser threshold measurements were carried out using segments of American Optical MG-702 neodymium-doped alkali silicate glass. This material has a lifetime of approximately 900 microseconds and an Nd_2O_3 concentration of 7 wt. percent. Because this lifetime is the longest of the materials investigated, the MG-702 glass is most easily pumped; for that reason, relatively more effort was devoted to this glass.

Because of the limited size of the available glass sample, a full disc could not be fabricated. However, we were able to produce a 1-3/8" wide central segment having a 3" diameter and a useful face area of about 20 cm^2. This segment was 1-cm thick and dielectric coated for 99.6% reflectivity at 1.06 micron wavelength on one face and low reflection coated on the opposite face.

The disc laser cavity was completed by addition of an external output mirror located 1 cm from the disc face.

Three types of measurements were carried out.

1. Laser threshold pump energy as a function of output mirror reflectivity.
2. Total laser output energy.
3. Near field laser energy distribution.

Laser threshold measurements were attempted using external mirrors with three different reflectivities. The results are given below:

TABLE F-I

Output Mirror Reflectivity	Threshold Input Energy
99%	190 joules
95%	1080 joules
85%	No laser action up to 3500 joules

The threshold indicated is the input energy delivered to the six FX-42 flash lamps in a 400 microsecond long pulse. These six lamps are uniformly spaced across a 3" x 3" plane. The maximum input energy capability of the experimental system (for a 400 microsecond pulse) was 3500 joules.

The laser output energy of the disc was measured by using a large diameter lens to focus the laser beam into a TRG laser calorimeter. At the maximum pump energy of 3500 joules and with a 95 percent reflectivity output mirror, the observed laser output was 1.1 joule. Since the pumping energy was a factor of three above the value at threshold, a significantly higher output was expected. Upon examination of the near field radiation from the laser segment, Fig. F1, it was found that the radiation came from only about 15 percent of the segment face. When averaged over this active area, the energy output density is 0.36 joules/cm^2. The streak nature of the lasing (Fig. F1) cannot be correlated with the pumping lamps whose long dimensions are orthogonal to the length of these streaks. However, the origin of the localized lasing can be inferred from the interferogram of the segment shown in Fig. F2. The optical distortion and the effects can be separated into two types described below.

a. First, there are about seven fringes across the segment which indicate a combination of an optical wedge and weak curvature distortion. These distortions are equivalent to an effective tilt and curvature deformation of the end mirrors of the cavity. From Part E we know that such deformations may easily introduce sufficient loss into a plane parallel Fabry-Perot resonator to prevent lasing.

b. Second, there are a number of strong localized stria. By observing the disc in a collimated gas laser beam, it was possible to determine that all of the stria had a positive cylindrical optical power. This lens action can modify the cavity locally to produce ar effective long radius "confocal" geometry (characteristic radius of curvature much longer than the mirror separation). This long radius "confocal" geometry is insensitive to the small tilt and the very long radius of curvature indicated by the widely separated fringes. Comparison of the interferogram and near field radiation revealed indeed that laser

Figure F1. Near Field Radiation from AO MG-702 Glass Segment

Figure F2. Interferogram of AO MG-702 Glass Segment

action was concentrated in areas containing strong stria. Although the wedge component of the plane parallel mirror deformation may be compensated for by tilting the external mirror, adjustment of that mirror failed to produce laser action in the areas between stria.

The importance of the confocal effect of the stria in reducing the threshold losses in the disc was verified in the following manner. Replacing the external plane mirror with a spherical mirror of 10 meter radius, it was found possible to obtain laser action in the regions of the segment free of stria where laser action could not be observed using plane mirrors. The threshold under these conditions was comparable to what was observed in the striaed areas when operating with a plane mirror.

The combination of the spherical mirror, and the plane mirror on the back face of the disc, forms a long radius confocal geometry with an effective spacing of 5 cm. When the near field laser pattern was observed, it was found to consist of a spot of ~0.7 mm diameter. This diameter is consistent with the theoretical predictions for this configuration.

In all these cases, it is so difficult to characterize quantitatively the cavity that any estimate of the total cavity loss is rather uncertain. For example, in a plane parallel geometry, we expect the narrow width of the lasing streaks to give rise to strong diffraction effects. However, to the approximation that we have an effective "confocal" geometry, we may expect diffraction losses to be very small. In any case, we can set a lower limit on the total loss per round trip since it is certainly greater than the sum of the following losses:

1. ~ 0.4% loss at each cavity mirror due to absorption and scattering
2. ~ 0.2% scattering loss for a double pass through the low reflection coated surface
3. transmission through the output mirror.

For the three values of output mirror transmission we have:

TABLE F-II

Output Mirror Reflectivity	Minimum Cavity Loss	Double Pass Gain Required for Threshold	Corresponding Inversion Level
99%	1%	0.043 dB	0.086 J/cm^2
95%	6%	0.254 dB	0.507 J/cm^2
85%	16%	0.750 dB	1.50 J/cm^2

The corresponding inversion is based on a gain coefficient of 0.25 dB/cm per joule/cm^3 inversion for the 900 μsec lifetime MG-702 glass.

Next we would like to see if these values of the inversion are compatible with the pump input energy. For a rectangular pump pulse, the maximum inversion level is given by:

$$N = P\tau \left[1 - e^{-T/\tau}\right] \qquad \text{(F1)}$$

where N = total inversion per cm^2 of disc face area (joules/cm^2)

P = effective rectangular pulse pumping rate (watts/cm^2)

τ = material lifetime (sec)

T = duration of effective rectangular pump pulse (sec)

For our oscillation experiments on the MG-702 glass, τ = 900 μsec and T = 400 μsec, so that Eq. F1 becomes

$$N = 3.24 \times 10^{-4} P \qquad \text{(F2)}$$

The effective pumping rate P can be written as:

$$P = CP'Q \qquad \text{(F3)}$$

where C = efficiency of conversion from input power to absorbed power

P' = lamp input power

Q = quantum efficiency, which is the fraction of the absorbed power that goes into inversion.

In Part D, measurements on energy absorbed in the laser disc as a function of lamp input energy P'T were described, and the results are plotted in Fig. D4. The conversion efficiency C can be obtained from Fig. D4. By assuming a value of 50 percent for Q, the effective pumping rate P can be calculated using Eq. F3. The effective pumping rate P as a function of lamp input power P' is plotted in Fig. F3.

With the aid of Fig. F3 and Eq. F1, the inversion N can be calculated for a 400 μsec long pump pulse for three oscillator conditions. The results are given in Table F-III. A comparison is made with the N obtained from Table F-II.

TABLE F-III

Output Mirror Reflectivity	Lamp Input Energy (Joules)	P' (Watts)	P (Watts/cm^2)	N (from Eq. F1) (Joules/cm^2)	N (from Table F-II) (Joules/cm^2)
99%	190	0.475×10^6	0.287×10^3	0.093	0.086
95%	1080	2.70×10^6	1.58×10^3	0.515	0.507
85%	3500	8.85×10^6	3.20×10^3	1.04	1.50

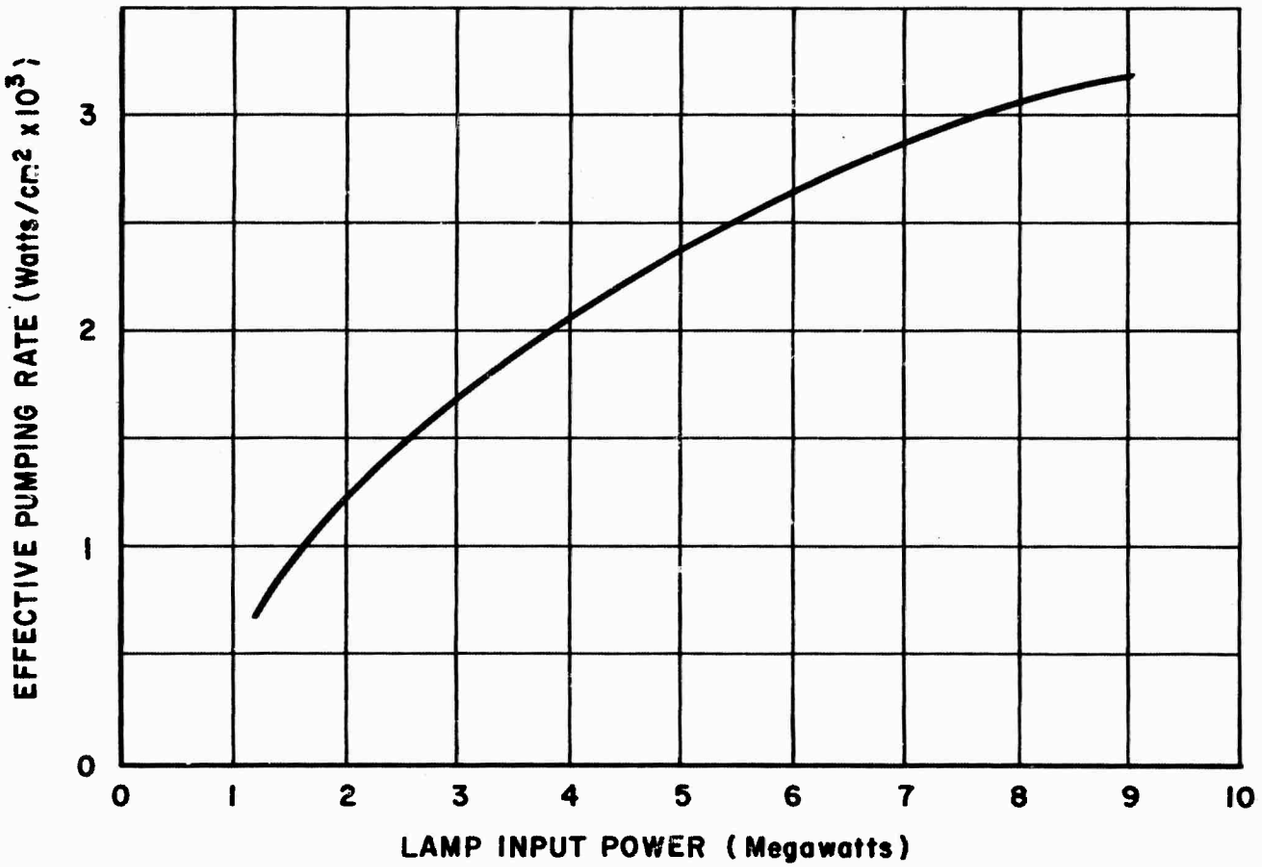

Figure F3. Effective Pumping Rate

We note that N from Eq. F1 is the inversion actually achieved, while N from Table F-III is the minimum inversion required for threshold. There is good agreement between the values of N in the upper two rows which indicates that the values of minimum cavity loss in Table F-II are very close to the actual total loss. The discrepancy between N's in the lowest row explains why threshold was not observed for that case.

Considering the good agreement between the threshold gain and pump absorption data, it is reasonable to extrapolate this to determine the inversion that can be obtained at maximum lamp loading. We were unable to carry out the threshold measurements at such a level at the time these experiments were being conducted since none of our larger power supplies was then available.

For a rectangular pulse of 10^{-3} sec. duration, the maximum input energy to the lamps is 9000 joules. This corresponds to an effective pumping rate (P) of 3.2×10^3 watts/cm^2.

Under these conditions, the maximum inversion that would be achieved is given by Eq. F1 with the following values for the parameters:

$$P = 3.2 \times 10^3 \text{ watts/cm}^2$$
$$\tau = 9 \times 10^{-4} \text{ seconds}$$
$$T = 10^{-3} \text{ seconds.}$$

Then $N = 1.92$ joules/cm^2 of disc area

For the MG-702 glass having a gain coefficient of 1/4 dB per joule of inversion this would indicate a single pass material gain of 0.48 dB or for the active mirror where we have a double pass through the material, a gain of 0.96 dB or 25 percent.

It should be noted that the calculated maximum inversion level is not indicative of the energy that can be extracted from the material since, in an oscillator, the threshold for laser action would be reached before this inversion was achieved; at this point, the laser process is the one governing the depletion of the metastable level rather than spontaneous decay. Since we are able to achieve a pumping ratio, i. e., the ratio of the maximum pumping rate to the threshold pumping rate (zero output), of over 10, we should realize an output of almost 3 joules per cm^2 of disc area in an oscillator configuration using the MG-702 glass.

OTHER GLASSES

1. American Optical AOLux-3835 - 5% Nd - 570 μsec Lifetime

No laser action could be produced in two discs of this glass. Although the optical quality of this glass appeared quite good, the disc surfaces, as

finished were not flat to better than 15 fringes. The discs were returned to American Optical for rework.

2. American Optical MG-403 - 5% Nd - 500 μsec Lifetime

No laser action could be produced in this glass. The optical quality was very poor. Interferograms indicated a high concentration of microscopic turbulent stria in addition to a major distortion of about 5 fringes. See Fig. A-2 in First Semi-Annual Technical Summary Report. (B1)

3. Eastman Kodak ND-11 - 6% Nd - 140 μsec Lifetime

This glass has provided us with the best optical quality of any of the laser glasses tested. Despite the high neodymium concentration, which resulted in appreciable concentration quenching and a short lifetime of 140 μsec, laser action was produced.

The threshold measurements on this 3" disc was carried out with a 400 μsec pump pulse and a 10-meter radius spherical output mirror. The threshold value was:

Mirror Reflectivity	Threshold Energy
99.6%	500 joules

Since the lifetime in this material is so short, further investigation was not undertaken.

4. Eastman Kodak ND-11 - 2% Nd - 360 μsec Lifetime

This glass was in the form of a six inch diameter disc with one inch in thickness. The disc was principally used for super-radiance and thermal distortion measurements since these effects are exaggerated by the large diameter. The optical quality was very good with less than 1/2 fringe distortion (at 0.63 μ wavelength) across the full aperture. Therefore, this disc was examined in the oscillator configuration to see if lasing could be achieved over a large area. At maximum pumping energy, examination of the near field radiation indicated rather uniform laser action over a single region covering about 1/3 of the face area. The lamp input energies at threshold for two plane output mirrors were:

Mirror Reflectivity	Threshold Energy
~ 99%	2500 joules
~ 95%	7500 joules

A large area of the dielectric mirror on the pumped face of the disc appeared to be damaged, which might explain the failure to achieve laser action across the full aperture. In addition, we have seen that 1/2 fringe distortion corresponding to $\sim\lambda/8$ at 1.06 μ wavelength could correspond to appreciable loss over much of the aperture. Since we did not intend to use this glass nor this 6" disc pumping assembly in the future, further investigation was not undertaken.

G. MODE SELECTION

Mode selectors have been used with lasers to produce a beam with divergence nearly equal to the diffraction limit. In many of these, pin-hole apertures have been used and the energy levels have been quite low. At higher energy levels, it is expected that the energy density in the pin-hole aperture may be so high that adverse effects such as breakdown may occur.

In devising a method of limiting the number of transverse modes that might be generated in the disc laser we have considered more seriously those techniques that do not require focusing the radiation to small areas producing destructive high energy densities. An attractive method is one first described by Collins and White[G1] using tilted etalons to limit the transverse modes in a ruby laser. By this method the mode selection or rejection can be carried out over the full laser aperture without the need for focusing the laser beam. This technique makes use of the fact that the optical frequency bandpass of an etalon structure, such as the disc, is dependent not only upon the optical thickness of the etalon but also upon the incident angle of the radiation.

INTRODUCTION TO TIPPED ETALON APPROACH

In the following analysis, the theory of a tipped etalon is discussed and applied to a laser. Mode selection is essentially a result of the transmission characteristics of a tipped etalon.

The ratio of transmitted to incident intensity for an etalon is given by Airy's Formulae:

$$\frac{I_t}{I_o} = \left(1 - \frac{A}{1 - R}\right)^2 \frac{1}{1 + \left(\frac{2F}{\pi}\right)^2 \sin^2 \frac{\delta}{2}} \qquad \text{(G1)}$$

where

R = power reflectivity at each face

A = power absorptivity at each face

λ = wavelength in vacuo of incident light

$F = \frac{\pi\sqrt{R}}{1-R}$, finesse of the etalon

$\delta = \frac{4\pi dn \cos\theta}{\lambda}$ = phase difference between a ray reflected directly from the front surface and a ray which reflects once off the back surface

θ = angle of refracted ray within etalon

d = thickness

n = index of refraction

n sin θ = sinØ (Snell's Law)

Ø = angle of incidence

Figure G1 shows how the transmittance (I_t/I_o) varies as a function of phase difference δ for two values of R. Since δ depends on the angle of incidence, a given etalon is strongly transmitting only in separated angular bands for incident monochromatic radiation. Let us place such an etalon inside a laser cavity and tip it with respect to the cavity axis. Consider the cavity to contain also a beam of finite angular width with its central ray parallel to the cavity axis. The rays which are incident upon the tipped etalon at angles exhibiting maximum transmittance will continue along the cavity axis with no loss due to reflection and a (usually) small attenuation due to the finite value of A. However, rays which are incident at other angles are partially reflected in a direction not along the cavity axis due to the tilt of the etalon. These reflected rays suffer high loss due to a combination of linear phase error and walk off (see Part E). Therefore only rays in narrow angular bands corresponding to directions of high transmittance through the tipped etalon suffer sufficiently small loss from the cavity to participate in the lasing phenomenon.

Figure G2 gives a schematic representation of the angular selectivity described above. Ray 1, parallel to the cavity axis, is incident with an angle $Ø_o$ at point 0 on the etalon in plane A. The concentric circles (seen as ellipses due to the perspective) in plane B define directions of maximum transmission for rays incident on the etalon at point 0. We show the etalon with a tilt angle $Ø_o$ corresponding to one of the directions of maximum transmission. Thus there is no reflected component for ray 1. Ray 2 is canted with respect to ray 1 through an angle $Ø_b$; we see from Fig. G2 that $Ø_b$ falls between the angles of maximum transmission and therefore ray 2 has a stongly reflected component ray 2". Of course any other ray parallel to ray 2 will be similarly reflected.

If the angle between the etalon normal and the direction of ray 2" is larger than $\sim 10^{-5}$ radians, then the loss per transit for the reflected beam will be quite high due to the linear phase error. (See Part E on Distortion Effects.) Under this condition we can consider the fractional loss per transit in the cavity due to etalon reflection to be given by

$$1 - \frac{I_t}{I_o} (Ø)$$

Figure G3 schematically shows I_t/I_o. The circles in the upper half define directions of maximum transmission for the etalon. The lower half shows an intensity profile as a function of angle. For an angle of incidence $Ø = Ø_o \pm \delta Ø/2$ the transmission is given by the primed expression $(I_t/I_o)'$. If the loss $1 - (I_t/I_o)'$ plus any other single transit losses is larger than the gain per transit arising from the active medium in the laser cavity and $Ø_b$ is the angular

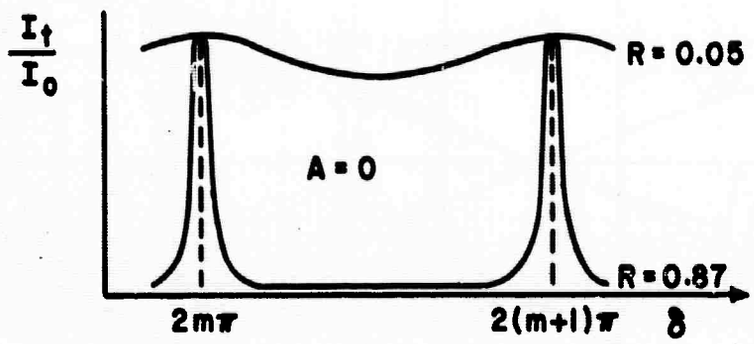

Figure G1. Transmittance of Etalon I_t/I_o vs Phase Difference δ for Two Values of Etalon Face Reflectivity

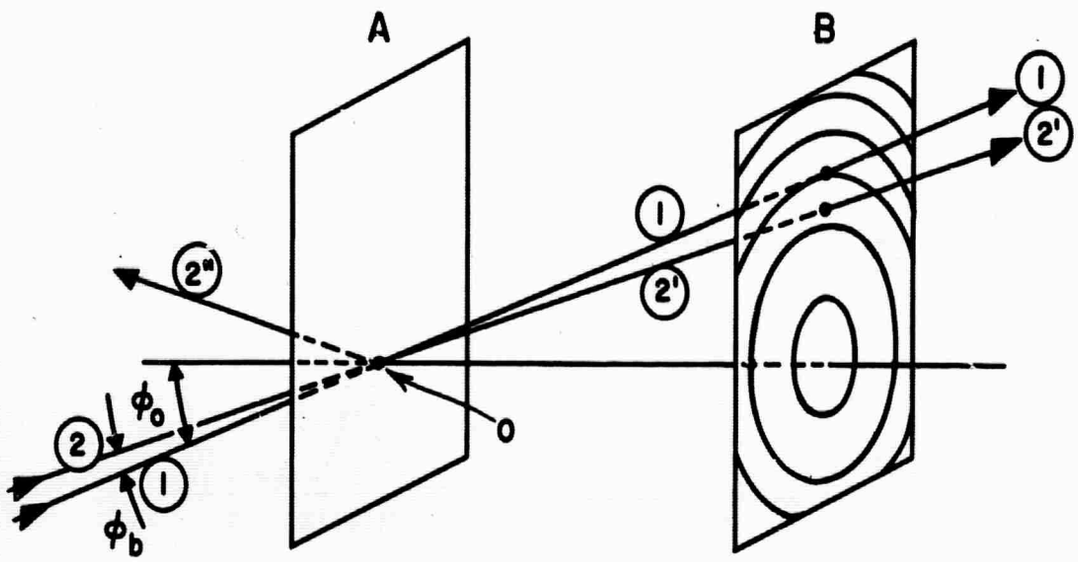

Figure G2. Schematic Representation of Angle Selective Transmission of Etalon

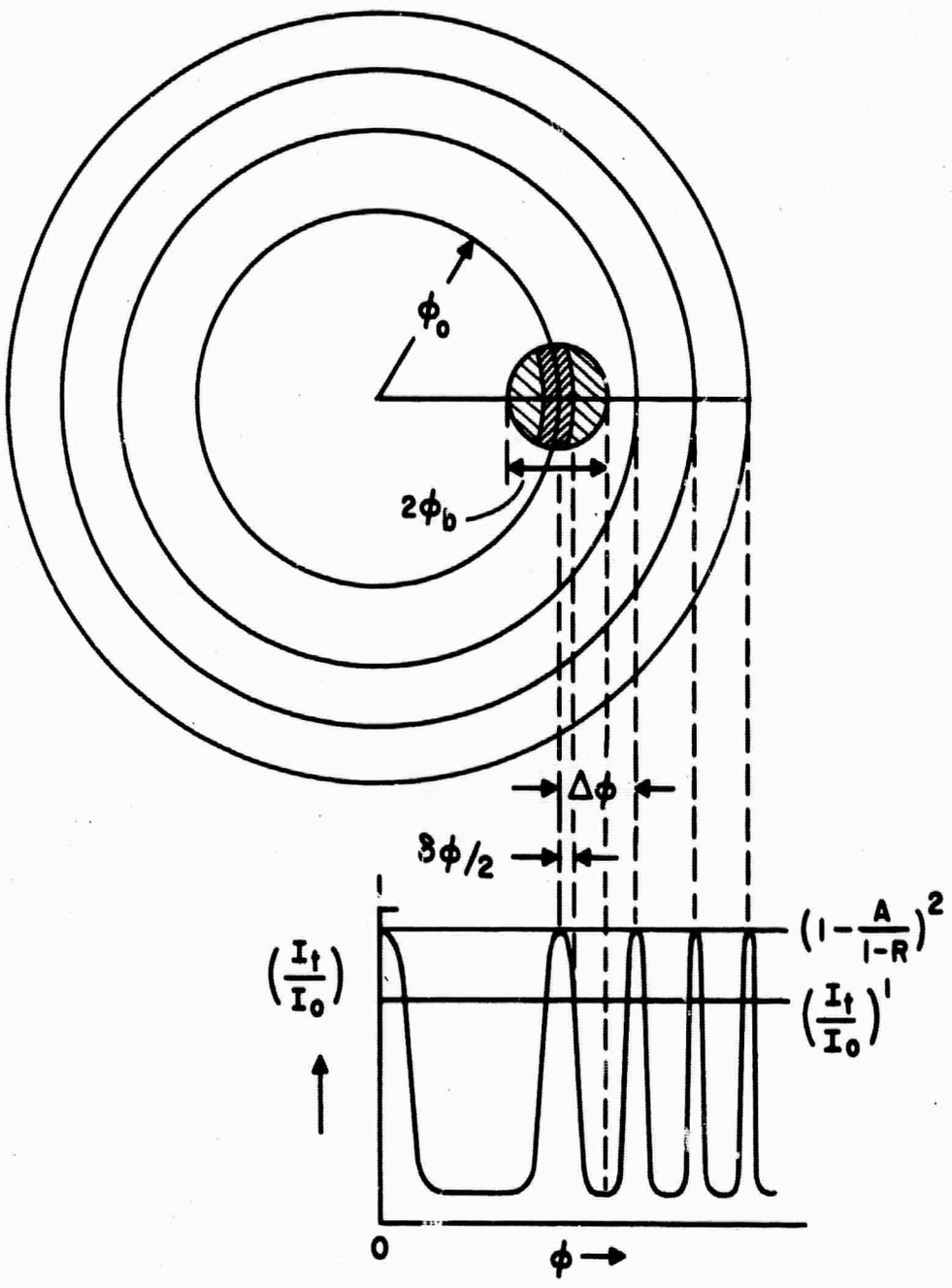

Figure G3. Schematic of I_t/I_o vs ϕ Curve and Its Relationship to Other Etalon Parameters

half width of the laser output beam without mode selection, then the half width of the output beam will be reduced from ϕ_b to $\delta\phi/2$. It should also be noted that the separation of the angular bands, $\Delta\phi$ must be greater than ϕ_b in order than only the central band of angles be favored for lasing. If $\phi_b > \Delta\phi$, then we would have more than one angular bands transmitted, each of a narrow width $\sim \delta\phi$ and separated by a broader width $\sim\Delta\phi$. Since these bands would tend to span the original beam width ϕ_b, no appreciable beam narrowing could be achieved with $\phi_b > \Delta\phi$. Thus one of the required characteristics of the tipped etalon mode selector is

$$\Delta\phi > \phi_b \tag{G2}$$

It is now clear that in order to design an etalon for narrowing the angular width of the laser output beam, we must have expressions for $\Delta\phi$ and $\delta\phi$ as functions of the etalon parameters and the loss required to prevent lasing. These expressions are developed in the next section.

THEORY FOR TIPPED ETALON MODE SELECTOR

From Eq. G1 we see that the condition on δ for I_t/I_o to be a maximum may be expressed as

$$\left(\frac{2F}{\pi}\right)^2 \sin^2\frac{\delta}{2} = 0$$

Then

$$\frac{\delta}{2} = \pm m\pi \text{ for maximum transmission} \tag{G3}$$

$$\frac{2dn}{\lambda}\cos\theta_m = m = \frac{2dn}{c}(\nu\cos\theta_m) \tag{G4}$$

We have added the subscript "m" to denote that the value of θ given by Eq. G4 is for the maximum in the transmission corresponding to the given value of m. Hence for a given value of mc/2dn, the compatible values of ν and θ for maximum transmission are given by:

$$\cos\theta_m = \frac{mc}{2dn\nu} = \frac{m\lambda}{2dn} \tag{G5}$$

For d = 2cm, n = 1.5, λ = 10,000 Å, solutions of Eq. G5 are plotted in Fig. G4.

Next, we calculate the values of the angle θ which are compatible with an arbitrary frequency ν and arbitrary value of $(I_t/I_o)/(I_t/I_o)_{max} = y$ for a given etalon[†]. The governing equation for this condition is easily seen from Eq. G1

[†]Of course y must be a solution of Eq. G1, i.e., $(I_t/I_o)_{max} \geq y \geq \dfrac{1}{1+\left(\frac{2F}{\pi}\right)^2}$

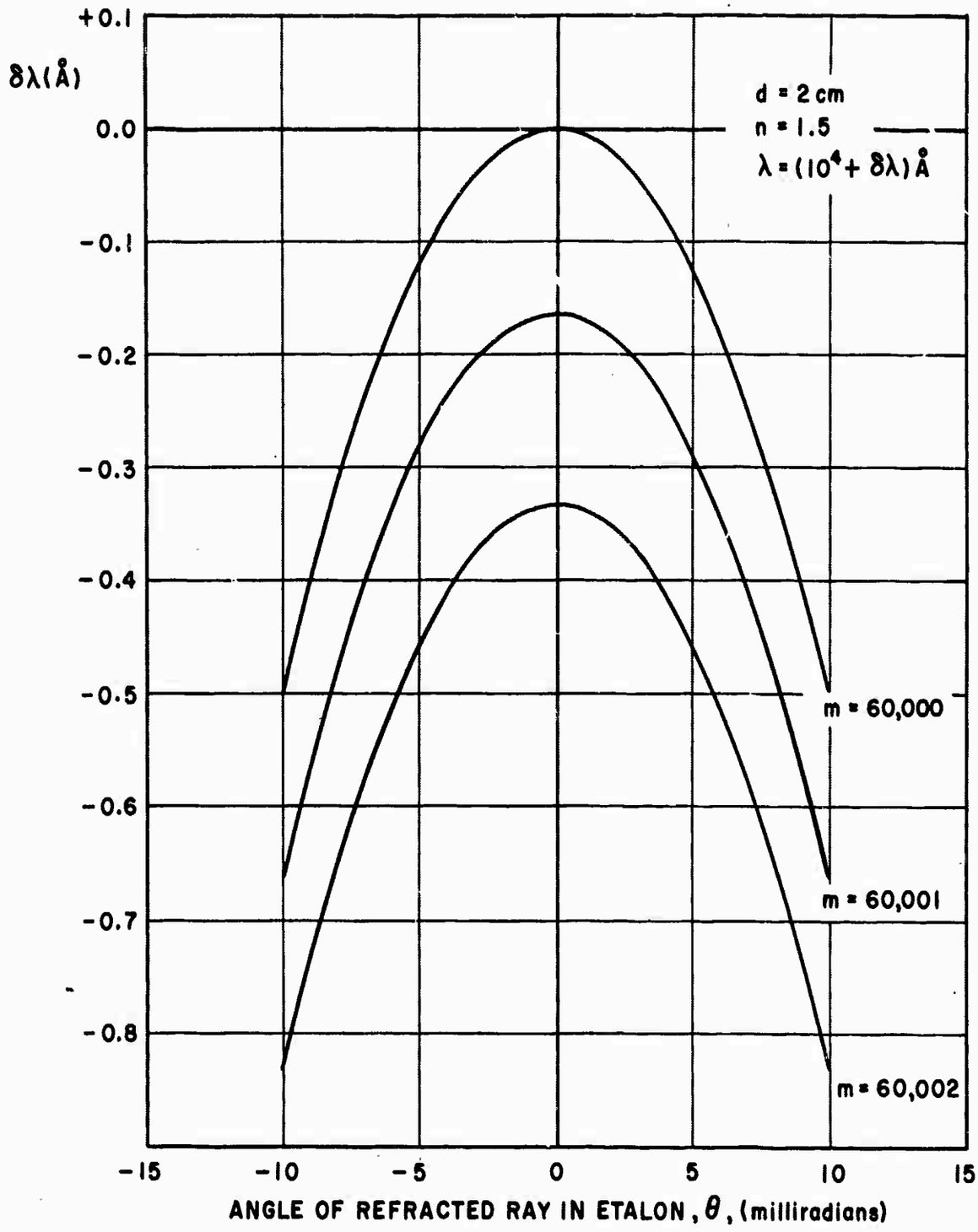

Figure G4. Tipped Etalon Transmission Characteristic

to be

$$\sin \frac{\delta}{2} = \pm \frac{\pi}{2F} \sqrt{\frac{1}{y} - 1} \equiv \pm x\pi \qquad \text{(G6)}$$

The parameter x which is related to y and defined in Eq. G6 can have any value between zero and $1/\pi$.

Assume:

$$\frac{\pi}{2F} \sqrt{\frac{1}{y} - 1} << 1 \qquad \text{(G7)}$$

or $\quad x\pi << 1$

Then, with Eq. G3,

$$\frac{\delta}{2} \pm \left\{ \begin{matrix} +m\pi + x\pi \\ +m\pi - x\pi \\ -m\pi + x\pi \\ -m\pi - x\pi \end{matrix} \right\} \equiv \pm m\pi \pm x\pi \qquad m = 0, 1, 2, \ldots$$

Thus from the definition of $\delta/2$ we have:

$$\frac{2dn \cos \theta}{\lambda} = m \pm x \qquad \text{(G8)}$$

Let us further assume that

$$\theta << 1 \qquad \text{(G9)}$$

Then

$$\frac{2dn}{\lambda} \left(1 - \frac{\theta^2}{2}\right) = m \pm x$$

$$\theta \doteq \pm \sqrt{2 - \frac{\lambda}{dn} [m \pm x]} \qquad \text{(G10)}$$

We note that for a real solution we require that:

$$2 - \frac{\lambda}{dn} (m \pm x) \geq 0$$

The reason for this is easily understood from consideration of Eq. G8. As m increases, cos θ must increase for a given λ, n, and d. However since cos θ cannot exceed unity there is a maximum value of m.

For a given value of $y = (I_t/I_o)/(I_t/I_o)_{max}$, the angular width $\delta\theta$ of the transmission band can be obtained from Eq. G10 and is given by

$$\delta\theta = \sqrt{2 - \frac{\lambda}{dn} [m - x]} - \sqrt{2 - \frac{\lambda}{dn} [m + x]} \qquad \text{(G11)}$$

We must remember that Eq. G11 is subject to the restrictions of Eqs. G7 and G9 which, however, can be easily realized. We may rewrite Eq. G11 with the aid of Eq. G5 and the small angle approximation (Eq. G9) as follows:

$$\delta\theta = \sqrt{2 - \frac{\lambda m}{dn} + \frac{\lambda x}{dn}} - \sqrt{2 - \frac{\lambda m}{dn} - \frac{\lambda x}{dn}} \qquad \text{(G12a)}$$

$$\delta\theta = \sqrt{\theta_m^2 + \frac{\lambda x}{dn}} - \sqrt{\theta_m^2 - \frac{\lambda x}{dn}} \qquad \text{(G12b)}$$

$$= \sqrt{\theta_m^2 + \theta_{mo}^2} - \sqrt{\theta_m^2 - \theta_{mo}^2} \qquad \text{(G12c)}$$

where

$$\theta_m^2 \doteq 2 - \frac{\lambda m}{dn}$$

$$\theta_{mo}^2 = \frac{\lambda x}{dn}$$

Next we note the value of $\delta\theta$ given by Eq. G12 becomes complex if $\theta_m^2 < \theta_{mo}^2$. The reason for this can be seen from consideration of Fig. G5. Thus for θ_m less than θ_{mo} we will choose an alternative definition of $\delta\theta$ as shown in Fig. G5. The two equations of $\delta\theta$ and the conditions are given below.

$$\delta\theta = \sqrt{\theta_m^2 + \theta_{mo}^2} - \sqrt{\theta_m^2 - \theta_{mo}^2}, \text{ if } \theta_m^2 = 2 - \frac{\lambda m}{dn} \geq \theta_{mo}^2 \qquad \text{(G13a)}$$

$$\delta\theta = 2\sqrt{2 - \frac{\lambda m}{dn} + \theta_{mo}^2}, \text{ if } 2 - \frac{\lambda m}{dn} \leq \theta_{mo}^2 \qquad \text{(G13b)}$$

$$\text{and } 2 - \frac{\lambda m}{dn} + \theta_{mo}^2 \geq 0$$

We note that in Eq. G13b we have avoided the use of θ_m since we cannot define a value of θ_m corresponding (same λ) to values of θ near the top of the curve given by

$$\theta = \sqrt{2 - \frac{\lambda m}{dn} + \frac{\lambda x}{dn}}$$

where $\theta \simeq 0$.

We conclude our discussion of $\delta\theta$ by noting an important limit when $\theta_m^2 \gg \theta_{mo}^2$:

$$\delta\theta = \frac{\theta_{mo}^2}{\theta_m} = \frac{\lambda x}{dn\,\theta_m}, \text{ if } \theta_m^2 \gg \theta_{mo}^2 \qquad \text{(G14)}$$

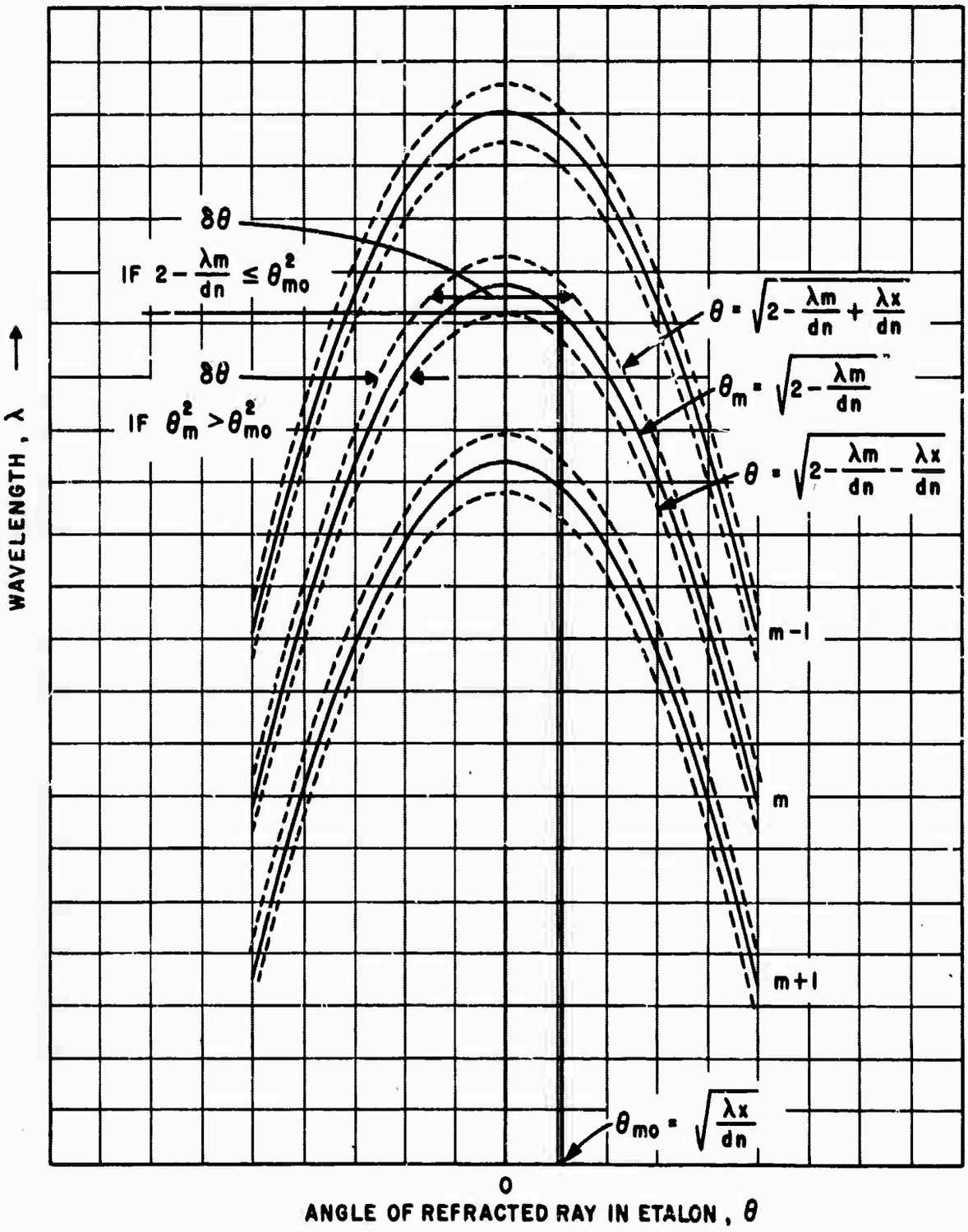

Figure G5. Diagram Showing Relation between $\delta\theta$ and θ_{mo}

Next let us calculate $\Delta\theta$, the separation between adjacent angular bands for a fixed frequency. We obtain the angular position of a transmission peak from either Eq. G5 with the small angle approximation, or Eq. G10 by letting $y = 1$ which means $x = 0$. Thus

$$\theta_m = \pm\sqrt{2 - \frac{\lambda m}{dn}} \tag{G15}$$

For a given positive value of θ_m, the angular position of the nearest transmission peak at the same value of λ is obtained by either a) increasing the integer m in Eq. G15 by unity, or b) using the minus sign and same value of m in Eq. G15, i. e., θ_m negative. We will find later that our interest will be in knowing the minimum value of $\Delta\theta$ so we define $\Delta\theta$ to be either of two quantities as follows:

$$\Delta\theta = \text{smaller of} \begin{cases} \sqrt{2 - \frac{\lambda}{dn}(m-1)} - \sqrt{2 - \frac{\lambda m}{dn}} \\ 2\sqrt{2 - \frac{\lambda m}{dn}} \end{cases} \tag{G16}$$

We may rewrite Eq. G16 by using again the small angle approximation of $\theta_m^2 \doteq 2 - \lambda m/dn$. Then

$$\Delta\theta = \begin{cases} \theta_m \left[\sqrt{1 + \frac{\lambda}{dn\theta_m^2}} - 1\right], & \text{if } \theta_m > \frac{1}{2}\sqrt{\frac{\lambda}{2dn}} \quad \text{(G17a)} \\ 2\theta_m, & \text{if } \theta_m < \frac{1}{2}\sqrt{\frac{\lambda}{2dn}} \quad \text{(G17b)} \end{cases}$$

The distinction between the two regions is illustrated in Fig. G6.

An interesting limit of Eq. G17a is

$$\Delta\theta = \frac{\lambda}{2dn\theta_m}, \quad \text{if } \theta_m^2 \gg \frac{\lambda}{dn} \tag{G18}$$

We note that corresponding to θ, an angle measured inside the etalon medium of index of refraction n, there is an angle outside the etalon, ϕ. It is easily shown that provided $\sin\phi \sim \phi$ and $\sin\theta \sim \theta$:

$$\phi = n\theta \tag{G19}$$

$$\delta\phi = n\delta\theta \tag{G20}$$

$$\Delta\phi = n\Delta\theta \tag{G21}$$

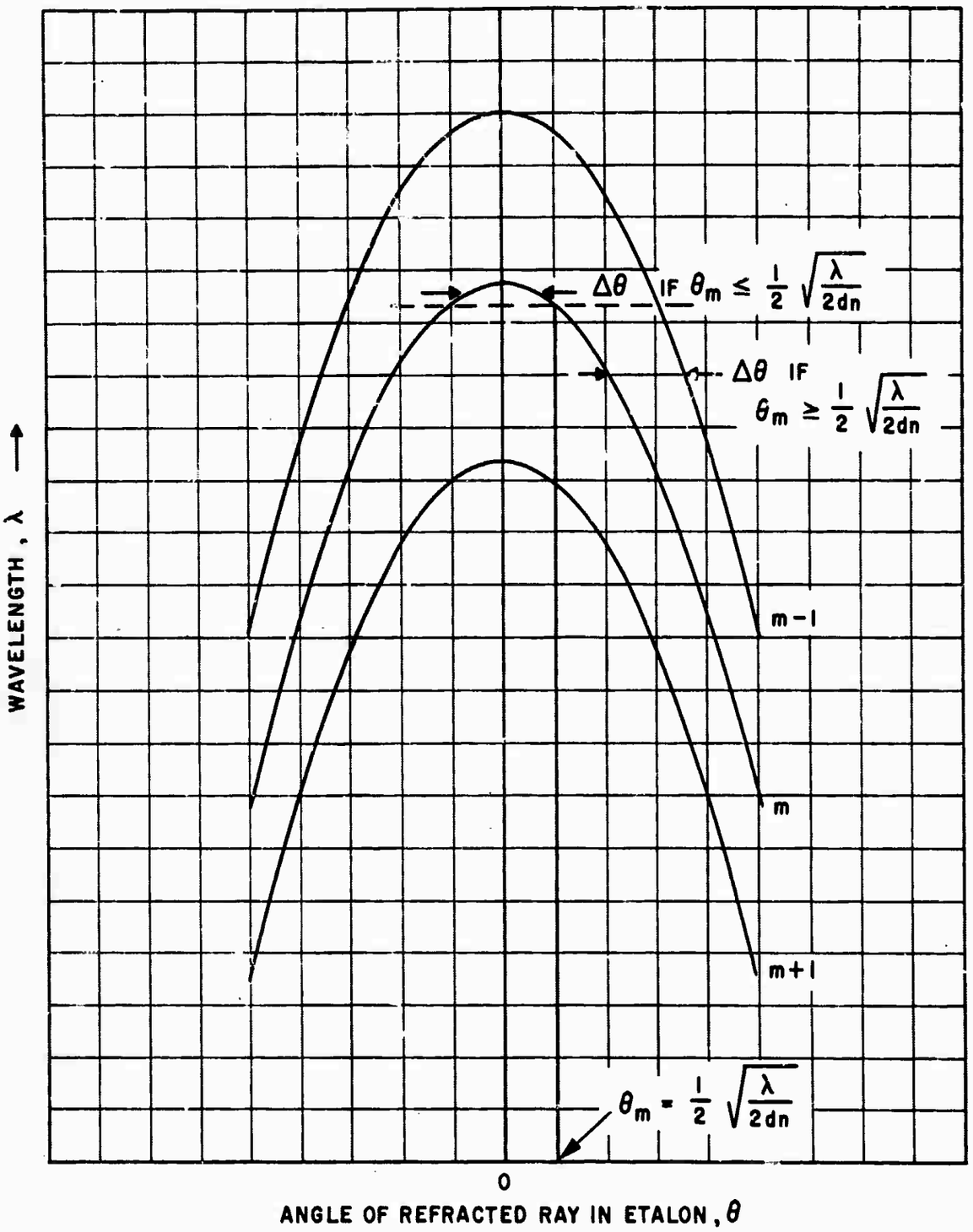

Figure G6. Diagram Showing Distinction between Two Definitions of $\Delta\theta$

DESIGN CONSIDERATIONS FOR TIPPED ETALON MODE SELECTOR

From our introductory remarks it is evident that the tipped etalon mode selector for beam narrowing should meet at least the following two requirements:

1) $\Delta\phi \gtrsim \phi_b$

2) $\frac{\delta\phi}{2}$, as small as possible, ideally approaching the diffraction limit, $\sim\lambda/D$, where D is the disc diameter.

The ideal situation where a diffraction limited beam is produced is not easily achieved in most situations so we will discuss several considerations which affect the choice of etalon parameters best suited to meeting the above two requirements.

In general we want $\Delta\phi$ to be sufficiently large so we can apply mode selection to lasers which (without mode selectors) produce a beam with half-width angle $\phi_b \sim \Delta\phi$ while at the same time we want the half-width of the mode selected beam $\delta\phi/2$ to be as small as possible. From Eqs. G13, G17, G20, and G21 we see that both $\Delta\phi$ and $\delta\phi$ depend upon θ_m so it is natural to seek the value of θ_m which produces the maximum ratio of $2\Delta\phi/\delta\phi$. If we consider the values of $\delta\theta$ and $\Delta\theta$ for large θ_m as expressed in Eqs. G14 and G18, then with the aid of Eqs. G20 and G21 we find

$$\frac{2\Delta\phi}{\delta\phi} = \frac{2\Delta\theta}{\delta\theta} = \frac{2F}{\sqrt{\frac{1}{y} - 1}} = \frac{1}{x} \qquad \text{if } \theta_m^2 \gg \frac{\lambda}{dn} \tag{G22}$$

It can in fact be shown that this limiting value is also the maximum value attainable when one varies θ_m.

Although the maximum value of $2\Delta\phi/\delta\phi$ is only attainable for large values of θ_m satisfying the inequality in Eq. G22, Fig. G7 shows that, provided one is willing to settle for $2\Delta\phi/\delta\phi$ being only <u>near</u> its maximum value, a considerably smaller value of θ_m is acceptable. For example, it is probably reasonable to accept 80 percent of the maximum value as a lower limit. Then we have from Fig. G7

$$\theta_m \geq 0.92\sqrt{\lambda/dn} \tag{G23}$$

A second lower limit on θ_m is provided by the requirement that the tilt of the etalon $\phi_m \simeq n\theta_m$ be sufficiently large so that the reflected light suffers total loss per transit. In practice, Eq. G23 provides the more stringent limit.

While Eq. G23 sets a lower limit to θ_m, the upper limit may be set by either of two effects. The first of these is the beam broadening effect illustrated in Fig. G8. Each internal etalon reflection makes the beam broader than its incident width W. This broadening gives rise to an effective loss since

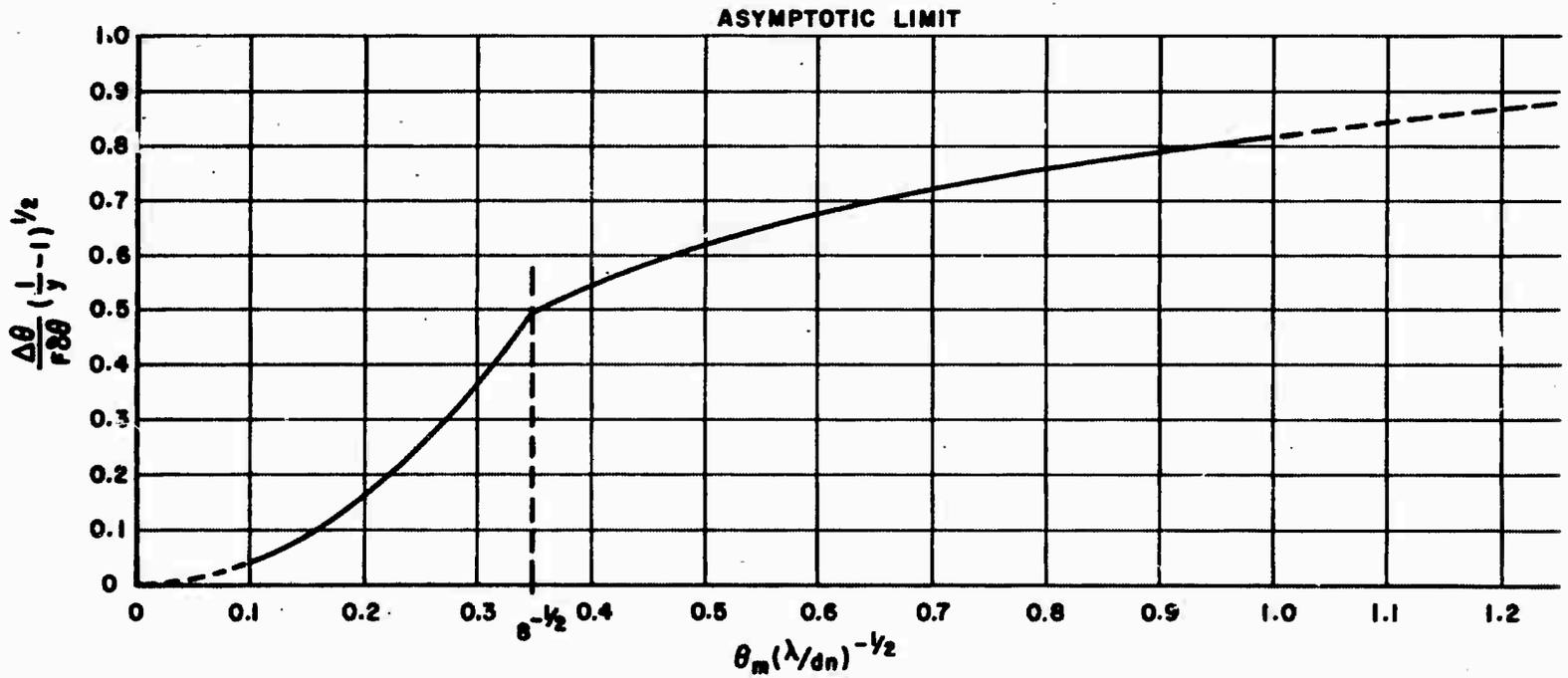

Figure G7. Graph Relating $\Delta\theta/\delta\theta$ to θ_m for Assumption that

$$\frac{\lambda x}{dn\theta_m^2} \ll 1$$

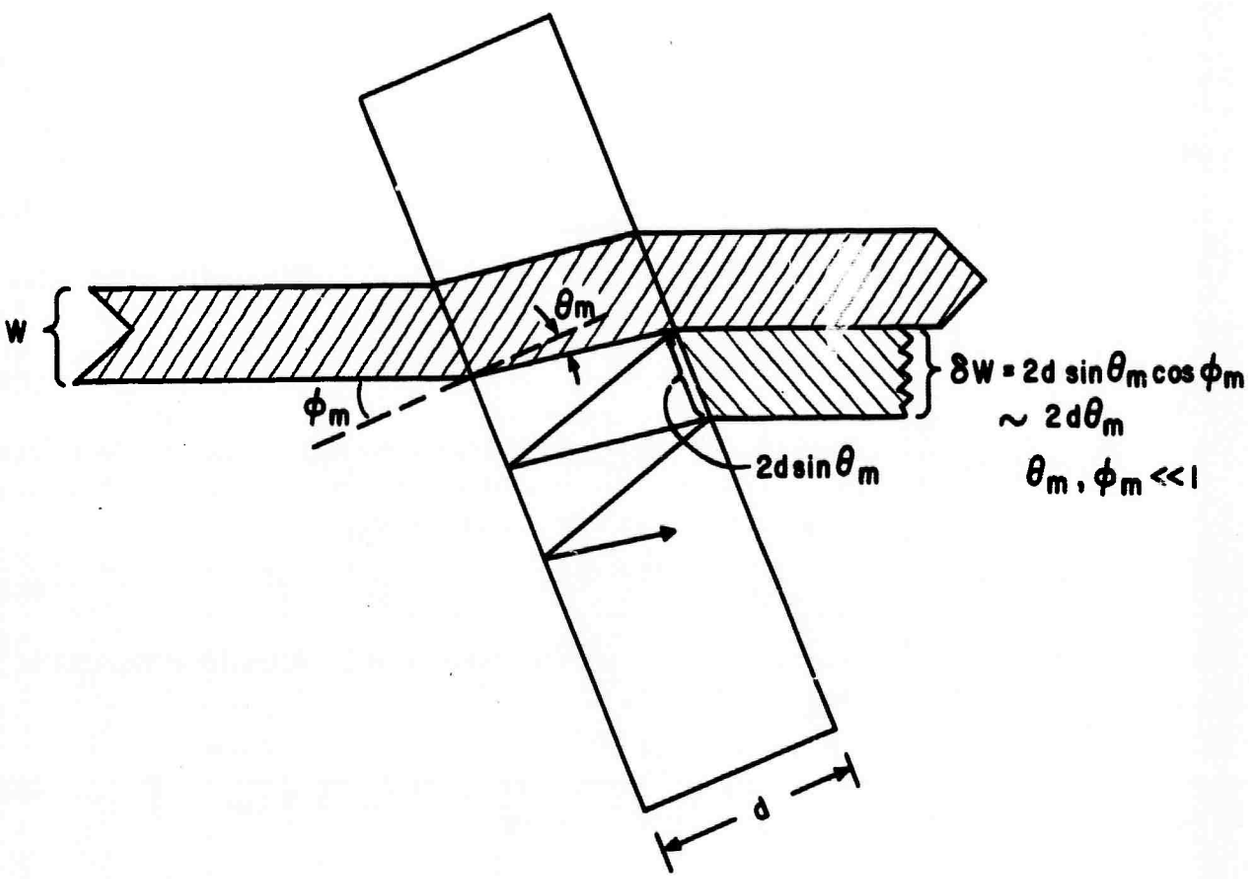

Figure G8. Beam Broadening within Tipped Etalon Due to Multiple Reflections

only the original width can match the active medium, receiving gain on each transit across the cavity. The total number of round trips in the etalon for one transit of the beam across the cavity is $\sim(1-R)^{-1}$. The effective loss per internal etalon round trip is $2d\theta_m/W$ in the small angle approximation. Therefore the loss per transit ℓ_{BBE} in the cavity due to beam broadening in the tilted etalon is:

$$\ell_{BBE} = \frac{2d\ \theta_m}{W\ (1-R)}, \quad (\theta_m \ll 1) \tag{G24}$$

Inverting, we have

$$\theta_m = \frac{D}{2d}\ (1-R)\ \ell_{BBE}, \quad \text{if } D = W \tag{G25}$$

Generally D is only slightly larger than W so Eq. G25 is usually valid. Because of physical rigidity requirements, it is desired that

$$\frac{D}{d} \leq 6 \tag{G26}$$

while ℓ_{BBE} must be some (usually small) fraction of the single transit cavity gain. The choice of R is dictated by considerations to be discussed below. Thus Eqs. G25 and G26 provide an upper limit to θ_m:

$$\theta_m \leq 3(1-R)\ \ell_{BBE} \tag{G27}$$

There is a second upper limit on the value of θ_m. Consider Eq. G17a which is repeated for convenience.

$$\Delta\theta = \theta_m \left[\sqrt{1 + \frac{\lambda}{dn\theta_m^2}} - 1\right], \quad \text{if } \theta_m > \frac{1}{2}\sqrt{\frac{\lambda}{2dn}} \tag{G17a}$$

By differentiating Eq. 17a we can show that $\Delta\theta$ decreases as θ_m increases. But we require that $\Delta\phi > \phi_b$ or equivalently $\Delta\theta > \phi_b/n$. Therefore we must have

$$\theta_m \left[\sqrt{1 + \frac{\lambda}{dn\theta_m^2}} - 1\right] > \frac{\phi_b}{n} \tag{G28}$$

which provides a second upper limit on θ_m.

From Eq. G22 it appears that we want the finesse F to be as large as possible. However, there is a conflicting consideration. A large value of F requires a high value of the face reflectivity R. But as R increases, the maximum transmission decreases as indicated by the following:

$$\left(\frac{I_t}{I_o}\right)_{max} = \left(1 - \frac{A}{1-R}\right)^2 \tag{G29}$$

Figure G9 shows a plot of $(I_t/I_o)_{max}$ vs R and also F vs R for different values of A. It is clear that if R or F is too large, the peak transmission will be reduced to the point where the cavity losses are unacceptably high. A realistic value for A (including scattering loss) for multilayer dielectric coatings is 0.005. Thus, for example, in order to keep the losses less than 2 percent at maximum transmission, we must have R less than 0.5. The optimum F and R will be a compromise between the requirements for a high degree of beam narrowing and the introduction of only small additional cavity losses.

A HYPOTHETICAL EXAMPLE

For a Nd disc which has a diameter of 7.5 cm we might choose an etalon with a diameter

$$D = 7.5 \text{ cm} \tag{G30}$$

For sufficient rigidity (see Eq. G26) let us choose

$$d = 2 \text{ cm} \tag{G31}$$

For a Nd laser we have

$$\lambda = 1.06 \times 10^{-4} \text{ cm} \tag{G32}$$

and a typical index of refraction for the etalon material is

$$n = 1.5 \tag{G33}$$

Assume that we will accept a 2 percent loss due to transmission through the etalon. Then for A = 0.005 we find

$$R = 0.5 \tag{G34}$$

$$F = 4.6 \tag{G35}$$

Next we determine the limits for θ_m which is assumed equal to the internal tilt angle. From Eq. G23 we have

$$\theta_m \geq 5.46 \times 10^{-3} \text{ rad.} \tag{G36}$$

With $\theta_m = 5.46 \times 10^{-3}$, Eq. G24 tells us that

$$\ell_{BBE} = 5.8 \times 10^{-3} \tag{G37}$$

which is a reasonably small value. For the same value of θ_m, Eq. G28 may be turned around to require that:

$$\phi_b < 3.9 \times 10^{-3} \text{ rad.} \quad (\sim \tfrac{1}{4} \text{ degree}) \tag{G38}$$

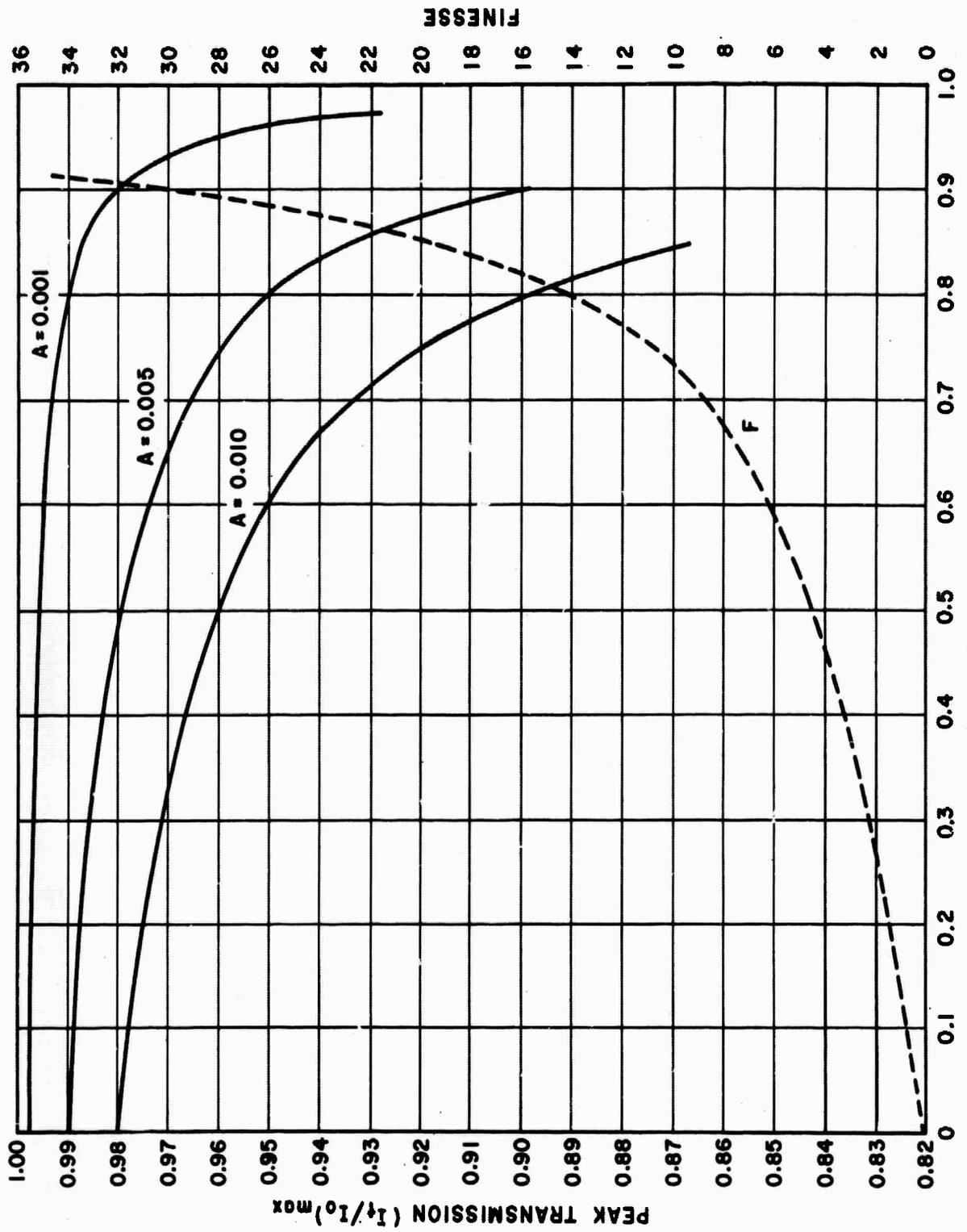

Figure G9. $(I_t/I_o)_{max}$ and Finesse vs Reflectivity of Etalon Faces

In summary a reasonable set of parameters for a beam narrowing tipped etalon is:

$D = 7.5$ cm

$d = 2$ cm

$\lambda = 1.06 \times 10^{-4}$ cm

$n = 1.5$

$R = 0.5$

$A = 0.005$

$F = 4.6$

$\theta_m = 5.46 \times 10^{-3}$ rad

Finally let us assume that $y = 0.90$. This says that an extra 10 percent loss will prevent lasing in undesired directions. Now we can calculate the amount of beam narrowing that may be achieved. Since $\theta_m > (1/2)\sqrt{\lambda/2dn}$, $\Delta\theta$ is given by Eq. G17a which yields:

$$\Delta\theta = 2.6 \times 10^{-3} \text{ rad}$$

Then

$$\Delta\phi = 3.9 \times 10^{-3} \text{ rad}$$

Since $\theta_m^2 \gg \lambda x/dn$, $\delta\theta$ is given by Eq. G14 which yields

$$\delta\theta = 2.4 \times 10^{-4}$$

Ther

$$\frac{\delta\theta}{2} = 1.2 \times 10^{-4} \text{ radians}$$

$$\frac{\delta\phi}{2} = 1.8 \times 10^{-4} \text{ radians}$$

Thus a beam with an angular half width less than 3.9×10^{-3} radians can be narrowed by a factor of 21.6 to a half-width of 1.8×10^{-4} radians.

ADDITIONAL PROBLEMS

First we note that a single tipped etalon only produces a strong angular narrowing of the beam in one direction. The reason for this is easily seen from consideration of Fig. G3. Therefore a pair of etalons with orthogonal planes of incidence must be used in order to significantly narrow the beam in two dimensions. These etalons must be carefully tuned to each other with

respect to their eigen-frequencies. The necessary precision of the frequency matching places severe requirements on the tolerances of the optical components with respect to alignment.

There are also severe tolerance requirements on the individual etalons with respect to flatness, parallelism, and other factors of optical quality. We have derived expressions for an ideal etalon but performance deteriorates rapidly as deviations from the ideal situation appear. For example, from Eq. G1 we see that the finesse of a perfect plane parallel etalon approaches infinity as the reflectivity goes to unity. However, if the etalon face is curved such that the optical thickness at the center of an etalon is $d + \lambda/q$ where d is the optical thickness at the edge, then Eq. G1 is not valid and the maximum finesse, F_{max}, no matter how large the reflectivity becomes, is $F_{max} = q/2$. (G1)
As another example we must be able to control and maintain the angular alignment of the tipped etalon to within ~50% of $\delta\phi$ (10^{-5} radians or ~2 seconds of arc for our specific etalon example).

We must also consider the relationship between the etalons' frequency characteristics and those of the laser cavity. We note that, for a fixed angle, the frequency separation between transmission or reflection peaks is given by

$$\Delta\nu = \frac{c}{2\,dn\cos\theta} \simeq \frac{c}{2dn} \qquad \text{if } \theta \ll 1 \tag{G39}$$

For fixed angle, the frequency separation of points on either side of the transmission peak exhibiting a transmission which is a fraction y of the peak transmission is given by

$$\delta\nu = \frac{\Delta\nu}{F}\sqrt{\frac{1}{y} - 1} \tag{G40}$$

Obviously $\Delta\nu$ and $\delta\nu$ are the analogues of $\Delta\theta$ and $\delta\theta$.

The most effective and efficient place to introduce mode selecting etalons is within the laser cavity. In this way, a portion of the energy which previously was directed off axis appears in the axial beam. In addition, you need only spoil the Q of the transverse waves a small amount in order to prevent their lasing if the discriminator is placed inside the laser cavity. However, you must severely attenuate the output in undesired directions if you place the discriminator outside the laser cavity. If we place tipped etalons inside the laser cavity, the latter's length must necessarily be longer than the etalon's thickness. This results, according to Eq. G39, in a smaller $\Delta\nu_c$ for the laser cavity than $\Delta\nu_e$ for the etalon. We have calculated $\Delta\theta$, the angular separation of the nearest transmission peak for a single, fixed frequency. However, if $\Delta\nu_c$ is less than $\Delta\nu_e$, then the nearest transmission peak is separated by an angle less than $\Delta\theta$ although the frequency of the nearest peak is different. We may overcome this difficulty by replacing the end mirror on the laser cavity by an axial mode selecting etalon (not tilted) whose frequency

characteristics essentially dominate the laser cavity. Then by properly matching eigen-frequencies of the cavity and etalon, we may realize the single frequency value of $\Delta\theta$ and such values of $\Delta\theta/\delta\theta$ as calculated earlier. Alternatively, one may choose to select axial modes by introducing additional tipped etalons of differing thicknesses.

CONCLUSIONS

It is difficult to evaluate the overall utility of this scheme for beam narrowing from consideration of our theoretical study alone. However, we have the experimental results of Collins and White[G2] to aid us. They have achieved a beam angle of approximately twice the diffraction limit using a ruby laser rod. There is a significant difference between their experiments and those in which we might employ tipped etalons. The ruby rod has a much higher gain than the Nd disc. Therefore the loss from etalon reflection required to prevent lasing is much higher with a ruby rod than with a Nd disc. Thus we may expect to achieve greater beam narrowing with the low gain disc system and approach the disc's diffraction limit which is smaller than that of the rod. The disadvantage of using two tipped etalons for beam narrowing is that this scheme introduces considerable loss into the laser cavity even for the most desirable mode. For a low gain system, the cost in terms of output energy may be substantial. This problem increases in severity as one attempts to achieve a higher degree of beam narrowing.

We see from our example that a substantial degree (> order of magnitude) of beam narrowing may be obtained by using tipped etalons with an additional cavity loss (~5%) per transit. However, the actual achievements of this method depend so strongly on the characteristics of the particular laser system in question, that they should be determined empirically. The theoretical studies carried out will provide valuable guidelines for such an investigation.

H. REFERENCES

B1 "Face Pumped Laser", General Electric Company, Semi-Annual Technical Summary Report, ONR Contract No. Nonr-4659(00), 1 December 1964 - 31 May 1965

B2 Paul Mauer, Eastman Kodak Co., private communication

B3 Fred A. Molby, "Optical Glasses", J. Opt. Soc. Am., Vol. 39, pp. 600-611, July 1949 (see Fig. 7, p. 609)

E1 J. Kotik and M. C. Newstein, "Theory of LASER Oscillators in Fabry-Perot Resonators", J. Appl. Phys., Vol. 32,pp. 178-186, February 1961

G1 Max Born and Emil Wolf, Principles of Optics, The MacMillan Co., New York (1959), p. 331

G2 S. A. Collins and G. R. White, "Interferometric Laser Mode Selector", Lasers and Applications, Ohio State University (1963), pp. 96-108